

# Power generation from sub-boiling geothermal wells using supercritical CO<sub>2</sub>



Author: Filip Vorobjov

Supervised by:

Erik G. Sogaard, Sigurd Solem, Kasia R. Arturi



## Acknowledgement

I am using this opportunity to express my gratitude to all those who have supported my throughout writing of this project, both family, friends, supervisors and colleagues.

I express a warm thanks to Sigurd Solem and Erik G. Sogaard for letting me work on this project and helped me with ideas in time of need.

A special thanks is dedicated to Jonas Solem for taking active participation the project, as with his help, constructive criticism and support a lot of progress has been achieved.



## Abstract

A number of experiments using supercritical CO<sub>2</sub> heat exchangers has been carried out in order to determine the most reliable heat transfer equation from the most commonly used. This was done by carrying out experiments, recording the data, and creating simulations based on the real system in a computing environment using Matlab and Fluidprop. After, the simulations were compared to experimental data, and an equation having the smallest RMSE compared to experimental data has been selected.

It has been found that the Gnielinski correlation, which is a modification of the Petukhov-Kirillov correlation gives an error of prediction of the fluid temperature of around 3 °C, when boiling water was used as the heating medium. It has also been determined that although the Gnielinski correlation is reliable in predicting the heat transfer coefficients between supercritical CO<sub>2</sub> and near/boiling water, when higher temperatures are used, or when the fluid is cooled down by using an ice bath, the correlation predictions are not reliable.

Using the information obtained from the experiments, a simulation of a power plant generating power from sub-boiling water hydrothermal wells by using a Rankine cycle with supercritical CO<sub>2</sub> has been created, optimized, and evaluated. By placing a U-tube heat exchanger on a 1000 m depth inside the hydrothermal well, and using common hydrothermal well parameters – 200 m<sup>3</sup>hr<sup>-1</sup>, 90 °C water flowrate through a 0.3 m diameter well, 600 MWhr<sup>-1</sup> theoretical power output has been achieved.

## Contents

Acknowledgement .....	3
Abstract .....	5
1 Aim of the Project.....	9
2 Background .....	9
2.1 Geothermal Energy.....	9
2.2 Thermal Energy.....	9
2.3 Carbon Dioxide .....	9
2.4 Supercritical Fluids.....	10
2.4.1 Natural Occurrence.....	10
2.4.2 Phase Diagrams.....	11
2.4.3 Applications of SCF.....	12
2.4.4 SCF in Power Generation.....	12
3 Geothermal Energy Extraction using Supercritical CO <sub>2</sub> .....	12
3.1 Supercritical CO <sub>2</sub> closed loop cycle .....	13
3.2 Dimensionless numbers .....	15
4 Fluid Mechanics.....	15
4.1 Fluid dynamics .....	15
4.1.1.1 Viscosity .....	15
4.1.1.2 Reynolds Number.....	18
4.1.2 Comparison of Friction Factors.....	22
4.1.3 Pressure loss .....	22
4.2 Adiabatic Fluid Compression .....	23
5 Thermodynamics .....	23
5.1 Equations of State.....	23
5.2 PR-EOS.....	24
5.2.1 Equations used in PR-EOS (26).....	24
5.3 Heat Transfer .....	25
5.3.1 Mechanisms of Heat Transfer.....	25
5.4 Heat Transfer Correlations .....	31
5.4.1 Nusselt Number based correlations.....	31
5.4.2 Non-Nusselt number correlations.....	32
6 Mechanical Design.....	33

6.1 Heat Exchanger Design .....	33
6.2 Material for construction .....	34
6.3 Positive Displacement Pump .....	35
6.4 Wall thickness calculation .....	36
7 Experimental Section .....	36
7.1 Development of the experimental apparatus .....	36
7.2 RMSE and errors of measurement .....	37
7.3 Parameter Verification .....	37
7.4 Experimental Procedure .....	39
7.5 Development of the algorithm .....	39
7.6 Results .....	40
7.7 Analysis .....	41
7.7.1 Petukhov-Kirillov .....	41
7.7.2 Gnielinski correlation .....	42
7.7.3 Dittus-Boelter .....	43
7.7.4 ESDU .....	44
7.7.5 Schwarz .....	44
7.8 Additional experiments .....	44
7.8.1 Experimental Results .....	45
7.8.2 Petukhov-Kirillov .....	46
7.8.3 Gnielinski .....	47
7.8.4 Dittus-Boelter .....	49
7.8.5 ESDU .....	50
7.8.6 Schwarz .....	50
7.9 Non-dimensionless numbers .....	50
7.10 Extreme Temperatures .....	52
7.10.1 Results .....	52
7.10.2 Petukhov-Kirillov .....	54
7.10.3 Gnielinski .....	56
7.10.4 Dittus-Boelter .....	57
7.10.5 Others .....	57
7.11 Inserted Thermocouples .....	57
7.11.1 Results .....	58

7.11.2 Analysis.....	59
7.12 Pressure Drop.....	64
7.13 Conclusion for the experimental section.....	64
8 Geothermal Plant Simulation.....	65
8.1 Simulation Requirements.....	65
8.2 Assumptions.....	65
8.3 System Specifications.....	66
8.4 System Performance.....	67
8.4.1 Transportation Pipes.....	67
8.4.2 Heat Exchangers.....	69
8.4.3 Grashof Number and Buoyancy Forces.....	73
8.5 Power output.....	75
8.6 Commissioning.....	75
8.7 Conclusion.....	76
References.....	77

# 1 Aim of the Project

The aim of the project is to develop and analyze the feasibility and stability of a novelty method of power generation from sub-boiling water geothermal wells using supercritical CO<sub>2</sub> as a heat carrier.

## 2 Background

### 2.1 Geothermal Energy

Geothermal Energy is Thermal Energy stored in the Earth. This energy originates from the original formation of the planet, as well as radioactive decay. The temperatures at the core-mantle boundary may reach over 4000 °C (1).

Geothermal energy in the form of hot springs has been used by humanity since Paleolithic times, and for space heating since ancient Roman times. However modern day use of geothermal energy is mainly for energy production. Based on data from 2013, 11.7 GW of geothermal power is produced worldwide (2). Geothermal power is cost effective, reliable, sustainable and environmentally friendly, but historically been limited to areas near tectonic plate boundaries.

The Earth's geothermal resources are theoretically more than enough to supply humanity's need for energy, however only a small fraction of the energy may be profitably exploited, as drilling and exploration for deep heat sources is very expensive.

### 2.2 Thermal Energy

Iceland is the world leader in direct geothermal heat applications. Around 92.5% of its homes are heated with geothermal energy, saving Iceland over \$100 million annually in oil imports. Reykjavik, once known as the most polluted city in the world, is now one of the cleanest (3).

Low temperature wells produce the energy equivalent of 100M BBL per year. These sources which produce water with a temperature of 30-150 °C, are normally used without conversion to electricity, but instead used for district heating, greenhouses, fisheries, industrial process heating, bathing. Home heating by means of geothermal energy is the fastest growing process of exploiting geothermal energy (4).

Low temperature wells are a lot more abundant and cheaper to drill for than high temperature ones. However there is a possibility to extract electricity from low heat geothermal wells by use of supercritical CO<sub>2</sub>.

### 2.3 Carbon Dioxide

Carbon Dioxide (CO<sub>2</sub>) is a colorless, odorless gas, vital to life on Earth. This is a naturally occurring chemical, which is composed of a carbon atom covalently bonded to two oxygen atoms. It is found in our atmosphere as a trace gas, at a concentration of about 400 ppm by volume (5).

Carbon Dioxide is used by the chemical, food and oil industries. It is used as a precursor chemical for synthesizing urea, methanol, and other products. In the food industry it is used for carbonating soft drinks, as well as infusing it in candy (Pop Rocks).

Another use of it in the food industry is decaffeination of coffee beans. To do this CO<sub>2</sub> needs to be in its supercritical state (6).

There are 2 main reasons as to why SC-CO<sub>2</sub> is used in decaffeination. The 1<sup>st</sup> one is that with varying pressure and temperature, SC-CO<sub>2</sub> exhibits selective solubility, which can be adjusted to extract almost pure caffeine from the coffee beans. The other reason is that CO<sub>2</sub> converts to supercritical state at

comparatively mild conditions – 31 °C and 73.9 bar. With such conditions it is quite easy to turn CO<sub>2</sub> supercritical and use its useful properties.

## 2.4 Supercritical Fluids

A supercritical fluid (SCF) is a substance which is subjected to a temperature and pressure higher than its critical point, where liquid and gas phases do not exist. They were discovered in 1822 by Baron Charles Cagniard de la Tour, while conducting experiments involving discontinuities of the sound of a flint ball in a sealed cannon barrel filled with various fluids at various temperatures (7). Supercritical fluids have no surface tension because they are not subject to vapor-liquid boundary, so no molecules have attraction to the interior of the fluid. The density and viscosity of a supercritical fluid are subjected to change when pressure and temperature are tampered with, and the SCF of a substance can have very different properties than the regular fluids. SCF can diffuse through solids like a gas, and dissolve materials like a liquid. Carbon Dioxide (CO<sub>2</sub>) and Water (H<sub>2</sub>O) are among the most commonly used SCF's, being used for decaffeination and power generation respectively (8).

### 2.4.1 Natural Occurrence

Supercritical Fluids are found in nature. One of the examples are underwater volcanoes, specifically those which are located deep beneath the ocean's surface, supercritical water is formed because of the immense pressure due to the depth and immense heat from the vents of the volcanoes.

The atmospheric pressure of Venus is approximately 90 times greater than that of earth, with an average temperature of 470 °C, and about 97 % of it is composed from CO<sub>2</sub>. This means it is reasonable to consider that the atmosphere of Venus is a supercritical fluid, because both the pressure and temperature exceed the supercritical parameters of CO<sub>2</sub>.

## 2.4.2 Phase Diagrams

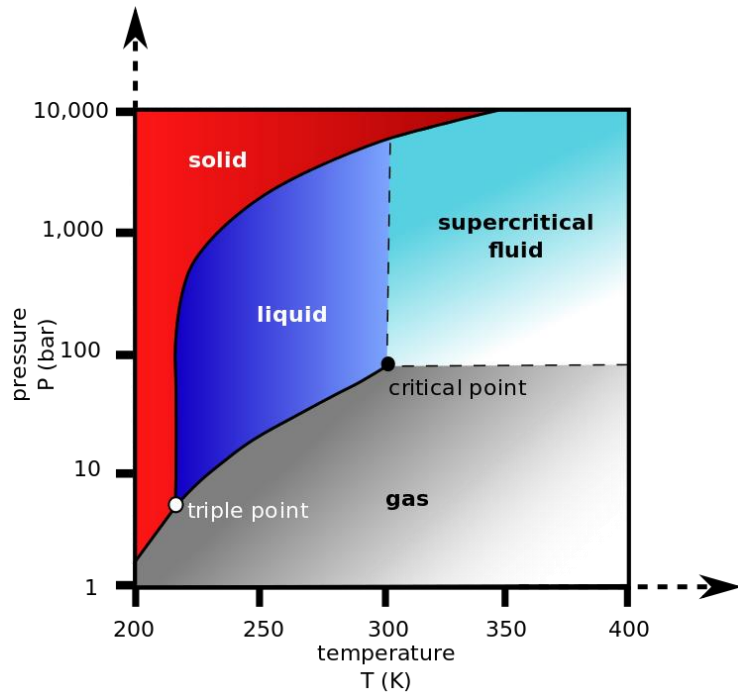


Figure 2.4.2.1

In the phase diagram (Figure 2.4.2.1) the boiling line separates the gas and liquid region, which ends with a critical point, where the gas and liquid phases unify into a single phase, called the supercritical phase. Depending on the pressure and temperature the supercritical fluid is subjected to, the fluid can behave more liquid or gas like.

<sup>1</sup> [https://en.wikipedia.org/wiki/Supercritical\\_carbon\\_dioxide](https://en.wikipedia.org/wiki/Supercritical_carbon_dioxide)

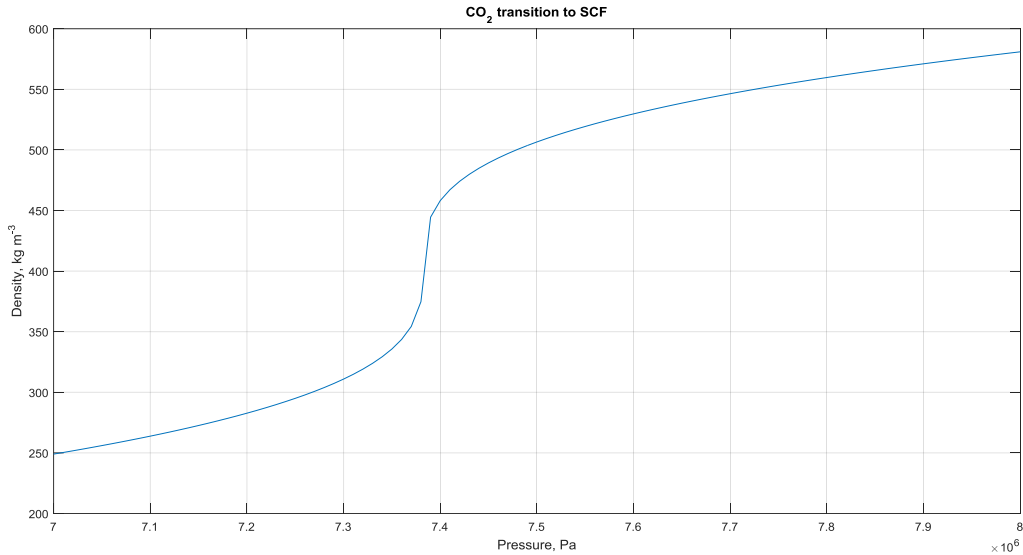


Figure 2.4.2.2

Figure 2.4.2.2 depicts CO<sub>2</sub> being compressed isothermally at its critical temperature of 314 K. It is clearly seen that at a pressure of ~7.4 MPa, where the critical point for CO<sub>2</sub> is located, a very sharp rise in density is detected, which corresponds to CO<sub>2</sub> transition from gas into a supercritical state.

### 2.4.3 Applications of SCF

The use of supercritical fluids today ranges from extraction of selected materials out of substrate, to applications in food science, and food ingredients, cosmetics, pharmaceuticals, polymers, nano-systems, fossils and biofuels, microelectronics, and biotechnology.

Extraction using SCFs is a fairly simple concept, much more efficient than normal extraction methods, which require heating and ventilation of solutions to the atmosphere. SCF's allow continuous extraction using common, inexpensive and non-toxic materials, and only requires venting to separate the extract out of the solution (9).

### 2.4.4 SCF in Power Generation

The efficiency of a heat engine is ultimately dependent on the temperature difference between the heat source and sink. This is called a Carnot Cycle. To improve efficiency of a power generating station, the operating temperature must be increased. Using water as the working fluid, this takes into account the supercritical conditions. Efficiencies can be raised from 39% (subcritical) to 45% (supercritical) using current technology (10). Supercritical Water Reactors are a promising technology in the nuclear industry. Carbon Dioxide can also be used in supercritical cycle nuclear power plants, with similar efficiency gains. However power generation using Carbon Dioxide is not only limited to nuclear power plants, but is also finding use for power generation in less extreme environments.

## 3 Geothermal Energy Extraction using Supercritical CO<sub>2</sub>

A novelty way was to produce electricity from sub-boiling water hydrothermal wells by means of supercritical CO<sub>2</sub> was proposed. The design is based on a closed loop Carnot cycle, which means that

temperature difference is the main driving force of the process.

The reason for selecting CO<sub>2</sub> as the heat carrier is due to its low supercritical point, and non-toxicity to the human body (11).

The main principle on which the system relies is the large variation of density with relatively small variations in pressure and temperature of the SC-CO<sub>2</sub>.

In the system, the CO<sub>2</sub> stays supercritical throughout the cycle. However to obtain maximum SC-CO<sub>2</sub> temperature difference, the SCF is pumped into the geothermal well. Due to the hydrostatic pressure, the pressure of the fluid increases, increasing its density. At a specific depth, a heat exchanger is located, which allows CO<sub>2</sub> to increase in temperature, which greatly decreases its density.

Below is an isobaric diagram, which shows how CO<sub>2</sub> density changes with temperature, and at a pressure of 12.8 MPa.

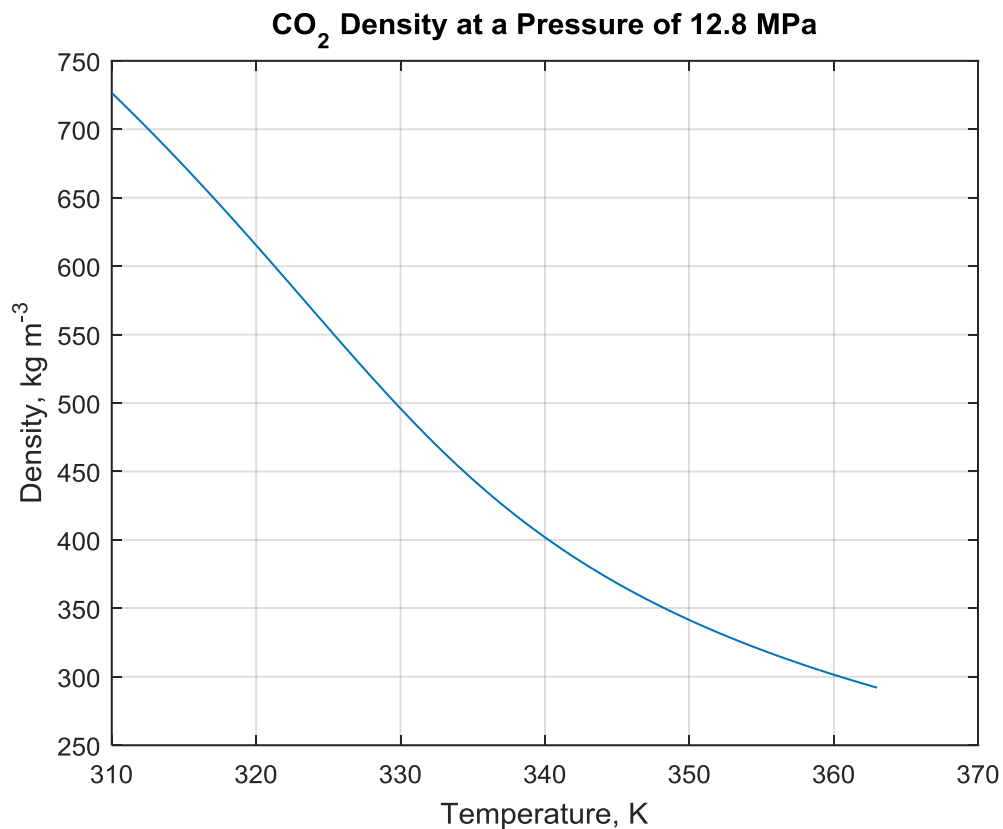


Figure 3.1

As it is seen from figure 3.1, an increase in temperature of about 50 K causes a drop in density of ~350 kg m<sup>-3</sup>. This fact can be exploited. As the pressure in the heat exchanger remains constant, but the density of the SC-CO<sub>2</sub> changes, buoyancy forces come into play, and the cold dense SC-CO<sub>2</sub> pushes out the less dense, hot SC-CO<sub>2</sub> to the surface. The pressure and temperature differences between the hot and cold sides of the cycle can then be exploited to generate electricity.

### 3.1 Supercritical CO<sub>2</sub> closed loop cycle

The technology that is to be developed can either be retrofitted to existing hydrothermal wells or installed into newly built wells. For this scenario, however, a case where the technology is retrofitted will be considered.

The system is model is based on a patent developed by Sigurd Solem, patent number **US 8,997,491 B2**.

The system starts by injecting CO<sub>2</sub> at supercritical conditions into an insulated pipe that's placed inside the well. The fluid then flows down the column, until it reaches the bottom heat exchanger. There the fluid absorbs the heat from the environment, changes its temperature, density, etc. and flows up another pipe up to the surface. Due to the fact that the fluid is hot it is less dense, therefore there will be a pressure difference at both sides of the columns (cold and hot). This pressure (and density) difference can be exploited by a positive displacement pump to extract energy from the process. Therefore the fluid is passed through a positive displacement pump (PDP), where its pressure is reduced. However after the PDP the fluid is still hot, and therefore a surface heat exchanger is required to lower the temperature of the fluid.

The schematic of the system is figure 3.1.1:

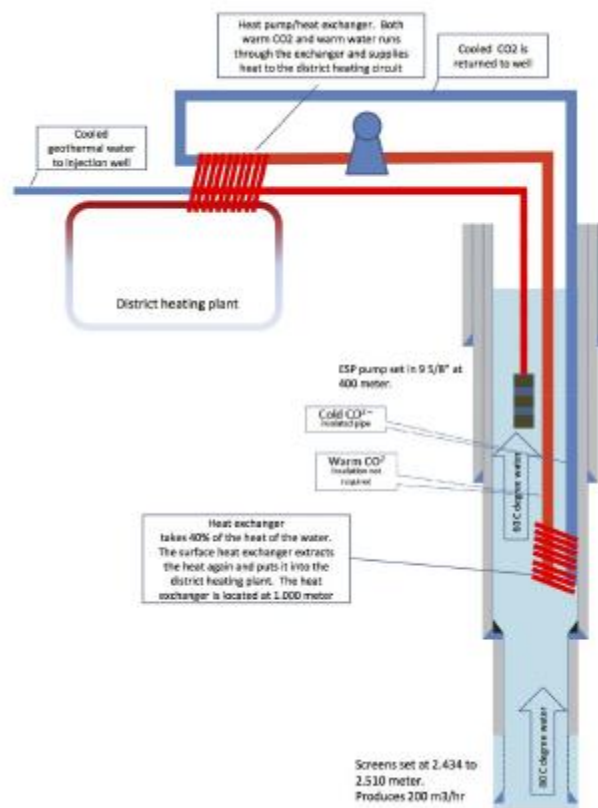


Figure 3.1.1

The physical limitation of the depth of the SC-CO<sub>2</sub> heat exchanger is set to be 1 km down, as that is the depth at which the hydro-pump is located at. At that depth the water temperature is 90 °C, and the pump operating capacity is 200 m<sup>3</sup> hr<sup>-1</sup>, with a well diameter of 30 cm.

This project focuses on a possibility of retrofitting a closed loop supercritical CO<sub>2</sub> Carnot cycle in order to determine if this process is economically viable.

### 3.2 Dimensionless numbers

In dimensional analysis, a dimensionless quantity is a quantity to which no physical dimension is applicable (12). Dimensionless quantities are widely used in many fields, such as mathematics, physics, engineering and economics. Dimensionless quantities are often obtained as products of ratios of quantities that are not dimensionless, but whose dimensions cancel in the mathematical operation. For the purpose of this project, a selection of dimensionless numbers will be introduced, which arise from analysis of fluid mechanics and thermodynamics.

## 4 Fluid Mechanics

Fluid mechanics is a branch of physics that studies mechanics of fluids, and forces that arise in them. The study of fluid mechanics goes back at least to the days of ancient Greece, when Archimedes investigated fluid statics and buoyancy and formulated his famous law, now known as the Archimedes principle.

Like any mathematical model of the real world, fluid mechanics makes some basic assumption about the materials being studied. Fluid mechanics must obey the following assumptions:

- Conservation of mass
- Conservation of momentum
- Conservation of energy

### 4.1 Fluid dynamics

This is a sub-discipline of fluid mechanics that deals with fluid flow. This sub-discipline offers a systematic structure, which underlies these practical disciplines – it embraces empirical and semi-empirical laws derived from flow measurement and used to solve real-life problems.

One of the most important properties of a fluid when its motion is considered is the viscosity.

#### 4.1.1.1 Viscosity

Viscosity calculations are possible due to semi-empirical series of equation described in a paper called 'Generalized Multiparameter Correlation for Nonpolar and Polar Fluid Transport Properties' (1988) (13).

The original equation provided by Chapman-Enskog theory (Chapman and Cowling, 1952) for diluted gas viscosity is written as:

$$\mu_0 = (4.0785 * 10^{-5}) \frac{\sqrt{MT} F_c}{V_c^{2/3} \theta^*}$$

However it only predicts dilute gas viscosity, and additional parameters are required to correct this equation to provide reliable data for dense gas viscosity predictions.

The factor  $F_c$  has been empirically found to be

$$F_c = 1 - 0.2756w + 0.059035\mu_\tau^4 + k$$

Where  $w$  is the acentric factor, and  $k$  is a correction factor for hydrogen bonding effect of associating substances (water, alcohol, acid). The term  $\mu_\tau$  is a dimensionless dipole moment. For non-polar gases only the two first terms are used in calculating  $F_c$ , since  $k$  and  $\mu_\tau$  in that instance turn to zero.

The  $\theta^*$  term is called the reduced collision integral, and it depends upon the intermolecular potential chosen.

$$\theta^* = \frac{A}{T^{*B}} + \frac{C}{\exp(DT^*)} + \frac{E}{\exp(FT^*)} + GT^{*B} \sin(ST^{*W} - H)$$

Where A, B, C, D, E, F, G, H, S and W are empirical constants, which are provided in table 4.1.1.1.1:

Constant	Value
A	1.16145
B	0.14874
C	0.52487
D	0.7732
E	2.16178
F	2.43787
G	-6.44E-04
H	7.27371
S	18.0323
W	-0.7683

Table 4.1.1.1.1

The dimensionless temperature  $T^*$  in this calculation is directly related to the potential energy parameter ( $\epsilon$ ), and Boltzmann's constant ( $\kappa$ ) by

$$T^* = \frac{kT}{\epsilon}$$

And the ratio between  $\epsilon$  and  $k$

$$\frac{\epsilon}{k} = \frac{T_c}{1.2593}$$

Therefore rearranging these two equations to cancel  $\epsilon$  and  $\kappa$ , and expressing in the form of  $T^*$  gives

$$T^* = 1.2593 \frac{T}{T_c}$$

For dense fluids the equation mentioned above does not apply, and an extended equation is required to take into account the effects for temperature and pressure that influence fluid viscosity. The equation takes the form of:

$$\mu = \mu_k + \mu_p$$

Where

$$\mu_k = \mu_0 \left( \frac{1}{G_2} + A_6 Y \right)$$

$$\mu_p = \left[ \frac{36.344 * 10^{-6} \sqrt{MT_c}}{V_c^{2/3}} \right] A_7 Y^2 G_2 \exp \left( A_8 + \frac{A_9}{T^*} + \frac{A_{10}}{T^{*2}} \right)$$

$$Y = \frac{\rho V_c}{6}$$

$$G_1 = \frac{1 - 0.5Y}{(1 - Y)^3}$$

$$G_2 = \frac{\frac{A_1(1 - \exp(-A_4 Y))}{Y} + A_2 G_1 \exp(A_5 Y) + A_3 G_1}{A_1 A_4 + A_2 + A_3}$$

Where

- $V_c$  - critical volume  $\text{cm}^3 \text{mol}^{-1}$
- $\rho$  – density in  $\text{mol cm}^{-3}$
- $M$  – molecular weight
- $\mu$  - viscosity in Poise

$A_1$ - $A_{10}$  are linear functions of the acentric factor ( $w$ ), reduced dipole moment ( $\mu_r$ ) and the association factor ( $\kappa$ )

$$A_i = a_0(i) + a_1(i)w + a_2(i)\mu_r^4 + a_3(i)\kappa, i = 1,10$$

However because this project is dealing with  $\text{CO}_2$ , which doesn't have a dipole moment or hydrogen bonding, the  $A_i$  simplifies to

$$A_i = a_0(i) + a_1(i)w, i = 1,10$$

The constants  $a_0$  and  $a_1$  were determined by regression of the viscosity data for non-polar fluids. The constants are given in table 4.1.1.1.2:

$i$	$a_0$	$a_1$
1	6.32402	50.4119
2	1.21E-03	-1.15E-03
3	5.28346	254.209
4	6.62263	38.0957
5	19.7454	7.63034
6	-1.89992	-12.5367
7	24.3	3.44945
8	0.79716	1.11764
9	-0.23816	6.77E-02
10	6.86E-02	0.34793

Table 4.1.1.1.2

Knowing the viscosity that the fluid processes it is possible to analyze the mode of fluid flow, using a dimensionless group called the *Reynolds Number*.

#### 4.1.1.2 Reynolds Number

In fluid mechanics, the Reynolds number ( $Re$ ) is a dimensionless quantity that is used to predict flow patterns in different fluid flow simulations (14).

Reynolds number is defined as the ratio of the momentum forces to viscous forces, and quantifies the relative importance of these forces for given flow conditions:

The Reynolds number is a function of the mass flow inside of the pipe and the pipe inside diameter:

$$u = \frac{\dot{m}}{\rho \left(\frac{D}{2}\right)^2 \pi}$$

$$Re = \frac{\rho u D}{\mu}$$

Where

- $\dot{m}$  - mass flow,  $\text{kg s}^{-1}$
- $u$  - velocity,  $\text{m s}^{-1}$
- $\mu$  - dynamic viscosity, Pa
- $D$  - pipe diameter, m

There are 2 types of flow that Reynolds number characterizes:

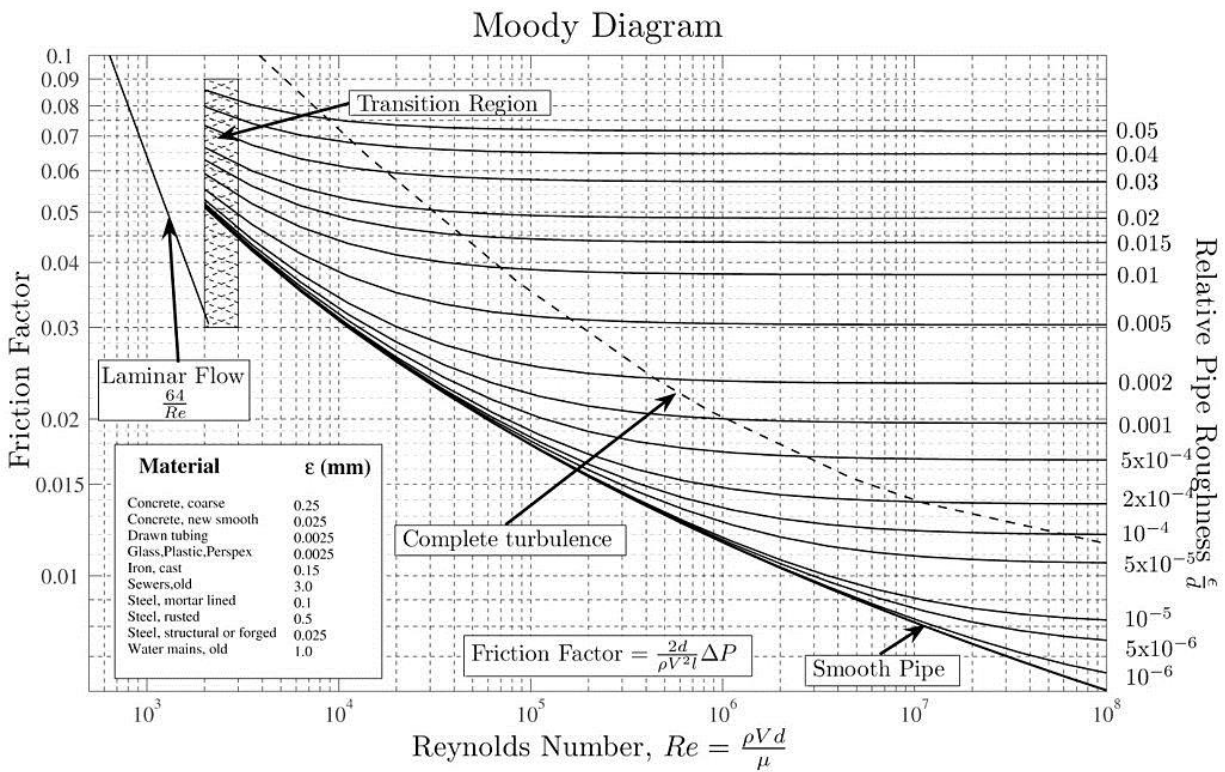
- Laminar flow, which occurs at low Reynolds numbers, where viscous forces dominate over momentum forces, and is characterized by smooth and constant fluid motion.
- Turbulent flow is dominated by inertial forces, which tend to produce random vortices, eddies, and other flow instabilities.

Although physicists managed to maintain a laminar flow regime for  $Re$  up to 100000 (Pfenniger, 1961), in most engineering cases the laminar flow can be considered to be stable for  $Re$  up to 2000, after which a transitional regime is observed. A transitional regime can be considered as laminar flow with instabilities, which if escalated can turn the flow turbulent. Generally turbulent regime is considered to be developed and stable at  $Re$  of around 4000.

In the context of this project only fluid flow within closed circular channels is considered (pipes). The flow of fluid through pipes causes various effects. One of the effects considered is the pressure drop, which is directly related to the friction factor.

#### 4.1.1.3 Friction Factor

Pressure loss in pipes is directly linked to pipe geometry (turbulent regime only) and Reynolds number. The pressure loss is determined by the use of a friction factor (Darcy or Fanning). This can be done either by the use of a Moody chart, or by a correlation that is used directly to find the friction factor (Colebrook-White equation) (15).



<sup>2</sup>Figure 4.1.3.1

As it is seen on the Moody chart (figure 4.1.3.1), when the flow is in laminar flow, the friction factor drops in a linear manner, which obeys the Poiseuille's law:

$$f = \frac{64}{Re}$$

<sup>2</sup> [https://en.wikipedia.org/wiki/Moody\\_chart#/media/File:Moody\\_diagram.jpg](https://en.wikipedia.org/wiki/Moody_chart#/media/File:Moody_diagram.jpg)

Which, as it is seen depends only on the Reynolds number, and is independent of the diameter (only friction of the fluid itself matters).

For turbulent regimes however, the friction factor is dependent on the diameter of the pipe and the relative roughness of the pipe compared to the diameter.

#### 4.1.1.4 Colebrook-White equation (16)

The Colebrook-White equation expresses the Darcy friction factor as a function of Reynolds number, pipe roughness and diameter.

$$\frac{1}{\sqrt{f}} = -2 \log \left( \frac{2.51}{Re \sqrt{f}} \right)$$

However this equation has unknowns (friction factor) on both sides of the equation, which means that the friction factor needs to be found iteratively. Therefore a number of equations have been developed to provide approximations to directly solve for the friction factor. A number of such equations are listed below.

#### 4.1.1.5 Goudar-Sonnard (17)

This is the most accurate approximation to solve directly for the Darcy friction factor for a full flowing circular pipe. The equation is the following:

$$a = \frac{2}{\ln(10)}$$

$$b = \frac{\varepsilon}{D}$$

$$d = \frac{\ln(10) Re}{5.02}$$

$$s = bd + \ln(d)$$

$$q = \frac{s}{s^2 + 1}$$

$$g = bd + \ln \frac{d}{q}$$

$$z = \ln \frac{q}{g}$$

$$D_{LA} = z \frac{g}{g + 1}$$

$$D_{CFA} = D_{LA} \left( 1 + \frac{\frac{z}{2}}{(g + 1)^2 + \frac{z}{3}(2g - 1)} \right)$$

$$f = \frac{1}{\left( a \left[ \ln \frac{d}{q} + D_{CFA} \right] \right)^2}$$

Where

- $\varepsilon$  – roughness height, (m)
- $D$  – Pipe diameter
- $Re$  – Reynolds Number

#### 4.1.1.6 Swamee-Jain (18)

Another equation to that can be used to predict the Darcy friction factor is the Swamee-Jain equation. This equation gives satisfactory results for engineering applications (the equation gives results accurate to 1%).

$$f = \frac{0.25}{\left[ \log_{10} \left( \frac{\varepsilon}{3.7D} + \frac{5.74}{Re^{0.9}} \right) \right]^2}$$

Where

- $\varepsilon$  – pipe roughness, m

#### 4.1.1.7 Petukhov (19)

Another equation friction factor equation has been developed by Petukhov (1958)

$$f = \frac{1}{(1.82 \log_{10} Re - 1.64)^2}$$

#### 4.1.1.8 Brkic solution (20)

Brkic shows one approximation of the Colebrook equation based on the Lambert W-function.

$$S = \ln \frac{Re}{1.816 \ln \frac{1.1Re}{\ln(1 + 1.1Re)}}$$
$$f = \frac{1}{\left( -2 \log_{10} \left[ \frac{\varepsilon/D}{3.71} + \frac{2.15S}{Re} \right] \right)^2}$$

The equation is said to match the Colebrook-White equation within 3.15%.

#### 4.1.1.9 Serghides's solution (21)

Serghides equation solves directly the Darcy-Weisbach friction factor for a full flowing circular pipe. The solution involves 3 intermediate values, which are later substituted into a final equation:

$$A = -2 \log_{10} \left( \frac{\varepsilon}{3.7D} + \frac{12}{Re} \right)$$
$$B = -2 \log_{10} \left( \frac{\varepsilon}{3.7D} + \frac{2.51A}{Re} \right)$$
$$C = -2 \log_{10} \left( \frac{\varepsilon}{3.7D} + \frac{2.51B}{Re} \right)$$

$$f = \frac{1}{\left(A - \frac{(B - A)^2}{C - 2B + A}\right)^2}$$

The equation was found to match Colebrook-White equation with an accuracy within 0.0023%.

#### 4.1.2 Comparison of Friction Factors

Since a large number of friction factor formulas are available for numerical simulations, the friction factors were compared by their accuracies. The reference equation was chosen to be the Goudar-Sonnad equation, since it is the most accurate approximation of the Darcy-Weisbach friction factor. For comparison, fully smooth pipes were chosen, with a relative roughness on zero. The following plot was generated:

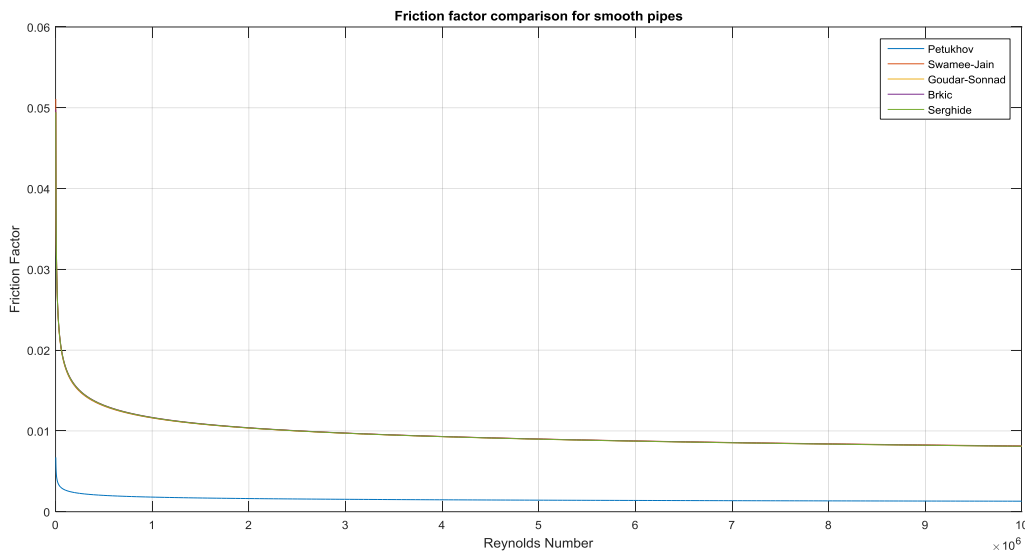


Figure 4.1.2.1

Figure 4.1.2.1 shows that apart from the Petukhov equation, all of the friction factor equations behave in the same way, therefore the Swamee-Jain equation has been chosen for simulation purposes, since computation wise it is the simplest equation.

#### 4.1.3 Pressure loss

After the friction factor is determined, the pressure loss in a full flowing circular pipe can be calculated, by use of the Darcy-Weisbach equation (22):

$$\Delta P = f \frac{Lu^2}{2Dg}$$

Where

- $g$  – gravitational constant,  $m\ s^{-2}$
- $L$  – length of pipe,  $m$

- $\Delta P$  – pressure loss, Pa

Finally, subtracting the pressure loss from the static pressure inside the column, the true pressure inside the pipe at given depth is obtained.

In addition to pressure loss, fluids (mainly gasses) experience compression in specific flow scenarios (compression in vertical downward flow, and decompression in upward vertical flow).

## 4.2 Adiabatic Fluid Compression

Having an assumption of perfectly insulated pipe (adiabatic process), fluid flowing down the pipe will experience compression, and this will result in a temperature increase of the fluid. This can be described by the following equation (23):

$$T_2 = T_1 \left( \frac{P_2}{P_1} \right)^{\frac{\gamma-1}{\gamma}}$$

$$\gamma = \frac{C_p}{C_v}$$

Where

- $C_p$  – Gas heat capacity at constant pressure, J mol<sup>-1</sup>
- $C_v$  – Gas heat capacity at constant volume, J mol<sup>-1</sup>

Adiabatic fluid compression is dependent on an internal fluid property such as heat capacity, which is a part of thermodynamics.

## 5 Thermodynamics

Thermodynamics is part of physics that deals with heat and temperature and their relation to energy and work. It describes such variables as internal energy, entropy, pressure, and partially describes thermal radiation. Thermodynamics describes bulk behavior of bodies, but not the microscopic constituents (molecules). The basic results of thermodynamics rely on the existence of idealized states of thermodynamic equilibrium. Lord Kelvin was the first person to formulate a concise definition of thermodynamics in 1854 (24):

*"Thermodynamics is the subject of the relation of heat to forces acting between contiguous parts of bodies, and the relation of heat to electrical agency."*

The macroscopic variables of a thermodynamic system in thermodynamic equilibrium, in which temperature is well defined, can be related to one another through *equations of state* (EOS).

### 5.1 Equations of State

In thermodynamics and equation of state is a relation between state variables (Pressure, Temperature, Enthalpy, Entropy, etc (25)). More precisely it is a set of equations that describe the state of matter given a set of physical conditions. These equations are useful in describing properties of fluids, mixtures of fluids, and solids.

Since 1873, when Van der Waal proposed his equation of state, many equations of state have been developed, some of which can be applied only in specific areas, some of which are more versatile than

the others, though still having their own constrains. For the purpose of this paper, the Peng-Robinson Equation of state will be considered only.

## 5.2 PR-EOS

PR-EOS was chosen because out of all general EOS it provides reasonably accurate data in a wide range of temperatures and pressures, and gives reasonable accuracy in predicting fluid density near its critical point.

### 5.2.1 Equations used in PR-EOS (26)

$$a = \frac{0.457235R^2T_c^2}{P_c^2}$$

$$b = \frac{0.077796RT_c}{P_c}$$

$$\alpha = (1 + k(1 - \sqrt{T_r}))^2$$

$$k = 0.37464 + 1.54226w - 0.26992w^2$$

$$T_r = \frac{T}{T_c}$$

$$A = \frac{a\alpha P}{RT}$$

$$B = \frac{bP}{RT}$$

$$Z^3 - (1 - B)Z^2 + (A - 2B - 2B^2)Z - (AB - B^2 - B^3) = 0$$

Where:

- R - 8.314 J (mol K)<sup>-1</sup> Universal Gas Constant
- P<sub>c</sub> – Critical Pressure, Pa
- P - Pressure, Pa
- T<sub>c</sub> – Critical Temperature, K
- T - Temperature, K
- T<sub>r</sub> – Reduced Temperature
- w – Acentric factor

The *a* and *b* terms are the attraction parameter and co-volume (volume of the molecules), respectively. The  $\alpha$  function in this case is a correction factor for vapor pressure prediction, which in turn is a function of both the temperature and acentric factor. The acentric factor is defined as the non-sphericity (centricity) of molecules. As it increases. The vapor curve is 'pulled' down, resulting in higher boiling points. The compressibility factor, *Z*, is calculated by implementing the *a* and *b* parameters into A and B,

which are correction factors, and arranging them into a polynomial form, the solution of which gives the compressibility factor of the system at given conditions.

Solving the polynomial for Z gives the compressibility factor. This in turn allows to predict the density of the fluid by the following equation:  $\rho = \frac{P \cdot M}{Z \cdot R \cdot T \cdot 10000}$ , which gives density in kg m<sup>-3</sup>.

As one of the most prominent used of an EOS is to correlate densities of gasses and liquids to temperatures and pressures, it can be used to predict fluid behavior when it experiences changes to internal energy (Heat Transfer).

### 5.3 Heat Transfer

Heat Transfer is the exchange of thermal energy between physical systems, depending on the temperature and pressure, by dissipating heat. Heat Transfer can occur by 4 different ways – conduction (diffusion), radiation, advection and convection.

Heat transfer always occurs from a region (body) with high temperature to a region (body) of lower temperature. This process changes the internal energy of both systems involved, and it's governed by the 1<sup>st</sup> law of thermodynamics:

*“In a thermodynamic process involving a closed system, the increment in the internal energy is equal to the difference between the heat accumulated by the system and the work done by it. (27)”*

Heat is defined as transfer of thermal energy across a well-defined boundary around a thermodynamic system. Heat transfer is a path function, as opposed to a function of state, therefore the amount of heat transferred through a thermodynamic process that changes the state of a system depends on how the process occurs, not only the difference between the initial and final states of the process.

Calculations of heat transfer by mechanical and thermodynamic means are done by a *heat transfer coefficient*, which is defined as the proportionality between the heat flux and thermodynamic driving force for the flow of heat.

Transport equations of thermal energy (Fourier's law), mechanical momentum (Newton's law for fluids), and mass transfer (Fick's law of diffusion) are similar, and analogies between these 3 transport processes have been developed to help to predict the conversion of one to another.

#### 5.3.1 Mechanisms of Heat Transfer

##### 5.3.1.1 Radiation

Thermal radiation is electromagnetic radiation which is generated by thermal motion of charged particles in matter. All matter at temperature above absolute zero emits thermal radiation (28). A common example of thermal radiation includes visible light.

Thermal radiation is different from convection and conduction – a person standing near an open fire experiences thermal radiation, although the surrounding air is cold.

The characteristics of thermal radiation depends upon various properties of the surface that emits in, such as temperature, spectral emissive power and absorptivity, as expressed by Kirchhoff's law. Thermal radiation of a body of a temperature greater than zero emits a wide range of frequencies. The frequency distribution obeys Plank's law of black body radiation (28). The dominant frequency (color) range of the body shifts to higher frequencies as the temperature of the body rises.

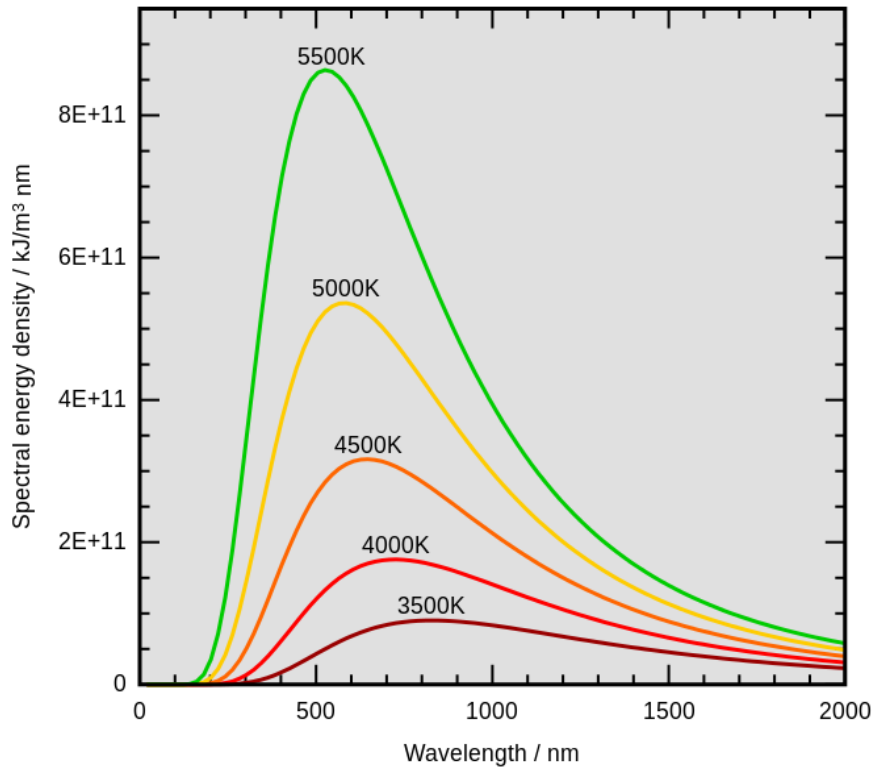


Figure 5.3.1.1.1

As seen on figure 5.3.1.1.1, the peak wavelength and total radiated amount of energy vary with temperature. And though this shows quite high temperature, the same relationship holds true for any temperature down to absolute zero.

The total amount of radiation of all frequencies increases steeply as the temperature rises. It grows as  $T^4$ , where  $T$  is the absolute temperature of the body. For example a stove in the kitchen about twice the room temperature on the absolute scale (600 K vs 300 K) will emit 16 times more radiation per unit area than the surroundings.

Because radiation is not relevant in this project it will not be discussed in detail further.

### 5.3.1.2 Advection

Advection is a transport mechanism of a substance of conserved property by a fluid due to the fluid's bulk motion. Sometimes advection and convection are used as synonyms, though convection covers transport by both advection and diffusion. Advective transport only describes the movement of a quantity by bulk flow of fluid (29).

### 5.3.1.3 Conduction

Conduction is the transfer of internal energy through collisions and diffusion of (quasi-) particles within a body or between contiguous bodies. This includes colliding molecules, atoms, electrons and photons. They transfer random kinetic and potential energy, which is jointly known as internal energy. Conduction occurs in all phases of matter – solids, liquid, gases and plasmas.

Conduction is a spontaneous process, where the heat flows within a body itself, unlike radiation, where heat can be transferred between objects separated by some distance apart.

In engineering, the conventional symbol for thermal conductivity is  $k$ . (In this paper it sometimes is referred to as  $\lambda$ )

### 5.3.1.3.1 Conductivity Equations

The fluid conductivity was is determined by utilizing the paper called 'Generalized Multiparameter Correlation for Nonpolar and Polar Fluid Transport Properties' (1988) (13).

Using a set of different equations, though still using a number of equations related to viscosity:

$$\lambda_0 = \frac{7.452\mu_0\varphi}{M}$$

$$\varphi = 1 + \alpha \left( \frac{0.215 + 0.28288\alpha - 1.061\beta + 0.26665Z}{0.6366 + \beta Z + 1.061\alpha\beta} \right)$$

$$\alpha = \frac{C_v}{R} - \frac{3}{2}$$

$$\beta = 0.7862 - 0.7109w + 1.3168w^2$$

$$Z = 2 + 10.5T_r^2$$

This equation however is only satisfactory for dilute gases, and in order to take into account temperature and pressure effects on the gas, another set of equations needed to be developed:

$$\lambda = \lambda_k + \lambda_p$$

Where

$$\lambda_k = \lambda_0 \left( \frac{1}{H_2} + B_6 Y \right)$$

$$\lambda_p = \left( 3.039 * 10^{-4} \frac{\sqrt{\frac{T_c}{M}}}{V_c^{2/3}} \right) B_7 Y^2 H_2 \sqrt{T_r}$$

$$H_2 = \frac{\frac{B_1(1 - \exp(-B_4 Y))}{Y} + B_2 G_1 \exp(B_5 Y) + B_2 G_1}{B_1 B_2 + B_2 + B_3}$$

Where

- $C_v$  – ideal gas heat capacity at constant volume cal (mol K)<sup>-1</sup>
- $R$  – gas constant – 1.987 cal (mol K)<sup>-1</sup>
- $\lambda$  – gas conductivity cal (cm s K)<sup>-1</sup>

The constants  $B_1$ - $B_7$  linear functions of the acentric factor ( $w$ ), reduced dipole moment ( $\mu_r$ ) and the association factor ( $\kappa$ )

$$B_i = b_0(i) + b_1(i)w + b_2(i)\mu_r^4 + b_3(i)\kappa; i = 1,7$$

But as with the calculation of viscosity, the terms for dipole moment and hydrogen bonding are reduced, so the final form of the equation is:

$$B_i = b_0(i) + b_1(i)w; i = 1,7$$

With the constants presented in table 5.3.1.3.1.1.

<i>i</i>	<i>b</i> <sub>0</sub>	<i>b</i> <sub>1</sub>
1	2.41657	0.74824
2	-0.50924	-1.50936
3	6.61069	5.62073
4	14.5425	-8.91387
5	0.79274	0.82019
6	-5.8634	12.8005
7	81.171	114.158

Table 5.3.1.3.1.1

#### 5.3.1.3.2 Prandtl Number

Prandtl Number (*Pr*) is a dimensionless number, which defines the ratio of momentum diffusivity to thermal diffusivity (conductivity).

$$Pr = \frac{C_p \mu}{k}$$

Where

- *C<sub>p</sub>* = fluid specific heat capacity, J kg<sup>-1</sup> C<sup>-1</sup>
- *k* = thermal conductivity W m<sup>-1</sup> K<sup>-1</sup>

Small values of Prandtl number means the thermal diffusivity dominates, whereas large values indicate that momentum diffusivity dominates the behavior. For example gasses have a low Prandtl number, which means that heat conduction is more significant compared to convection, so thermal diffusivity is dominant. Engine oils, however have a high *Pr*, which means convection is more effective in energy transfer (30).

#### 5.3.1.4 Convection

Convective heat transfer (sometimes referred to simply as convection) is the transfer of heat from one place to another by the movement of fluids. It is normally the dominant form of heat transfer in liquids and gasses. Although it is discussed as a distinct method of heat transfer, convective heat transfer involved the combined processes of conduction and advection (31).

Convection can be described as natural (buoyancy forces) or forced by movement of a fluid by means other than buoyancy forces. Thermal expansion of fluids may also force convection. An example of this can be a draft from a chimney. Natural convection arises from difference in density of hot and cold fluids. A common example of this can be heating water in a pot, where hot water rises from the bottom of the pan, displacing the cold fluid, which flows downward. Without the presence of gravity though, natural convection does not occur, and only forced convection is in action.

### 5.3.1.5 Buoyancy force (32)

Natural, or buoyancy convection is a very important mechanism that operates in a variety of environments, ranging from cooling electric circuits, to large scale circulation of fluids in oceans, and the atmosphere. It is caused by the action of density gradients, in conjunction with gravitational fields.

There are 2 scenarios in the context of natural convection. In one, a density gradient exists in a fluid in a direction that is parallel to the gravity vector, or opposite to it. Such situations can lead to 'stable' or 'unstable' density stratification of the fluid. In a stable stratification, the less dense fluid is at the top, and denser fluid at the bottom. In the absence of other effects, convection will be absent, and we can treat the heat transfer problem as one of conduction. In an unstable stratification, in which the less dense fluid is at the bottom and denser fluid is at the top, provided the density gradient is sufficiently large, convection will start spontaneously, and significant mixing of the fluid will occur. This is easily visualized in figure 5.3.1.5.1:

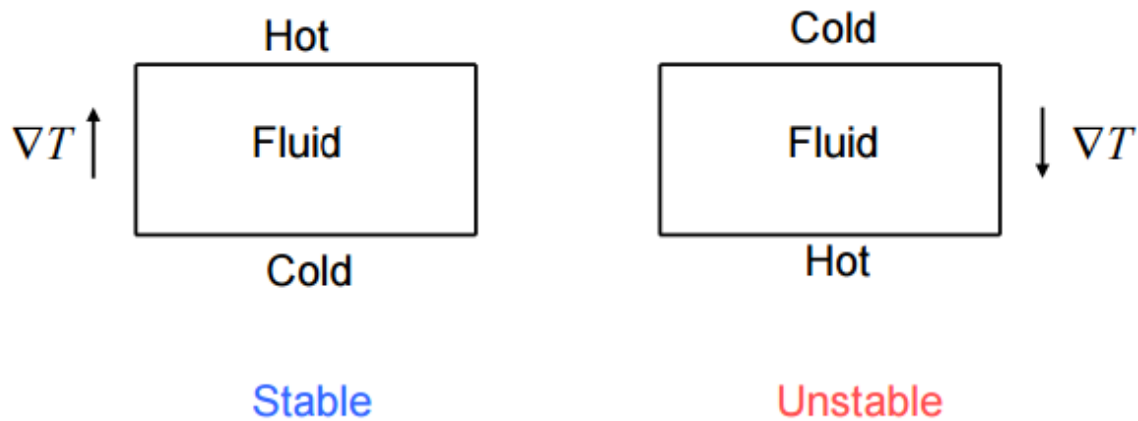


Figure 5.3.1.5.1

It is worthwhile to note that density gradients may arise not only because of temperature differences, but also from composition gradients, even in an isothermal system. However for the purpose of this project the composition gradient is not applicable due to the fact that only  $\text{CO}_2$  is used.

#### 5.3.1.5.1 Grashof Number

In natural convection situations, an important dimensionless group is the Grashof Number ( $Gr$ ) (32). To provide some physical significance to this group, we use a simple order of magnitude estimate of the natural convection velocity. When a fluid with a density  $\rho$  moves at a velocity  $V$ , the kinetic energy per unit volume can be written as  $\frac{1}{2}\rho u^2$ . This must come from some other form of energy, namely the potential energy lost by the fluid. Over a distance  $L$ , the difference in potential energy between the less dense fluid in the boundary layer and a more dense fluid outside can be approximately expressed as  $g\Delta\rho L$ , where  $g$  is the gravitational constant, and  $\Delta\rho$  is the density difference between the boundary layer and fluid that is far away. It is possible to equate these two order of magnitude estimates, and neglect the factor of  $\frac{1}{2}$ , because it's only an order of magnitude analysis.

$$\rho u^2 \approx g\Delta\rho L$$

And therefore, a typical order of magnitude of the velocity arising from natural convection is

$$u \approx \sqrt{\frac{\Delta\rho}{\rho} gL}$$

Now it's possible to define Reynolds number for the flowing fluid using this order of magnitude estimate.

$$Re_L = \frac{Lu}{\mu} = \sqrt{\frac{\Delta\rho}{\rho} gL^3}$$

So the  $Re^2 = \frac{\Delta\rho gL^3}{\mu^2}$ . This is a dimensionless group that occurs often in natural convection problems, and is defined as the Grashof Number.

It is then possible to relate fluid convection velocity through the Reynolds and Grashof number:

$$u = \frac{\sqrt{Gr}\mu}{\rho d}$$

Where

- $\Delta\rho$  – Density difference,  $\text{kg m}^{-3}$
- $g$  – Gravitational constant ( $9.81 \text{ m s}^{-2}$ )
- $L$  – Characteristic length (m)
- $d$  – Pipe internal diameter (m)

#### 5.3.1.6 Convective heat transfer

The equation that governs heat transfer by convection is (33):

$$q = hA(T_a - T_b)$$

Where:

- $q$  – heat transferred per unit time
- $A$  – area of heat transfer
- $T_a$  – objects surface temperature
- $T_b$  – fluid temperature

##### 5.3.1.6.1 Relationship between conduction and convection (Nusselt Number)

Nusselt Number ( $Nu$ ) is the ration of convective to conductive heat transfer across the boundary. In this context, convection includes both advection and diffusion. A Nusselt number close to one (convection and conduction of a similar magnitude) is a characteristic of a laminar flow. Larger Nusselt numbers correspond active convection, with turbulent flow is typically in the 100-1000 range (34).

$$Nu = \frac{hL}{k}$$

Where

- $h$  = convective heat transfer coefficient  $W\ m^{-2}\ K^{-1}$
- $L$  = characteristic length  $m$
- $k$  = thermal conductivity  $W\ m^{-1}\ K^{-1}$

Since there are methods available to calculate thermal conductivity of gasses, the Nusselt number can be used to calculate the convective heat transfer coefficient. A number of equation has been developed to calculate the Nusselt Number.

## 5.4 Heat Transfer Correlations

Below are presented selected heat transfer equations that are going to be examined on their performance in simulations in comparison with experimental data.

### 5.4.1 Nusselt Number based correlations

#### 5.4.1.1 Petukhov Kirillov Correlation

For supercritical fluids a modified equation is provided by Petukhov and Kirillov (1958) (35)

$$Nu = \frac{\frac{f}{8} Re Pr}{K_1 + K_2 \sqrt{\frac{f}{8}} \left( Pr^{\frac{2}{3}} - 1 \right)}$$

Where  $f$  is the friction factor (Petukhov), and  $K_1$  and  $K_2$  are correction factors that are expressed as

$$K_1 = 1 + 3.4f, K_2 = 11.7 + 1.8Pr^{\frac{1}{3}}$$

The given equation is said to give prediction of  $Nu$  with a maximum error of about 2%.

Range of applicability:  $0.5 < Pr < 2000$ , and  $10^4 < Re < 10^6$

#### 5.4.1.2 Dittus-Boelter correlation (36)

The earliest correlation for turbulent heat transfer in a smooth tube was provided by Dittus and Boelter. A common form to be used for fluids with Prandtl number in the range of  $\approx 0.7-100$ , and tubes with  $L/D > 60$ .

$$Nu = 0.023 Re^{0.8} Pr^n$$

Where  $n=0.4$  for heating a fluid, and  $n=0.3$  if the fluid is being cooled.

Range of applicability:  $0.6 < Pr < 160$ , and  $10^5 < Re$

#### 5.4.1.3 Gnielinski correlation (36)

An equation that is similar to Petukhov and Kirillov was developed by Gnielinski. This equation extends the range of applicability into transitional regimes.

$$Nu = \frac{\left(\frac{f}{8}\right) (Re - 1000) Pr}{1 + 12.7 \sqrt{\frac{f}{8}} \left( Pr^{\frac{2}{3}} - 1 \right)}$$

Where  $f$  is the same friction factor developed by Petukhov.

Range of applicability:  $0.5 < Pr < 2000$ , and  $3000 < Re < 5 \times 10^6$

#### 5.4.1.4 Schmidt Correlation (37)

Schmidt (1967) developed a correlation that's applicable for turbulent in heat exchangers, which is applicable from the critical Reynolds number up to  $Re \leq 22000$ . The critical Reynolds number in a coil heat exchanger depends on the curvature of the pipes, and more specifically the ratio of the radius of the pipe to the radius of the coil.

$$\delta = \frac{r}{R}$$

$$Re_{crit} = 2300[1 + 8.6\delta^{0.45}]$$

$$Nu = 0.023 \left[ 1 + 14.8(1 + \delta)\delta^{\frac{1}{3}} \right] Re^{[0.8+0.22\delta^{0.1}]} Pr^{\frac{1}{3}}$$

Where

- R – coil diameter, m
- r – pipe radius, m

Range of applicability:  $Re_{crit} < Re < 22000$

#### 5.4.2 Non-Nusselt number correlations

An alternative method to determine the convective heat transfer coefficient is by the use of another dimensionless group, the *Stanton Number*.

##### 5.4.2.1 Stanton Number (38)

Stanton number (*St*) is a dimensionless number that characterizes the intensity of energy dissipation in a liquid or gas flow. It is also used to characterize heat transfer in forced convection flows. It can also be represented in terms of the Nusselt, Prandtl and Reynolds numbers.

$$St = \frac{Nu}{RePr} = \frac{h_i}{\rho u_t C_p}$$

Stanton number arises from the consideration of the geometric similarity of the momentum and thermal boundary layers, where it can be used to express a relationship between the shear force, as well as the heat transfer at the wall.

##### 5.4.2.2 ESDU correlation

The equation is provided by the Engineering Sciences Data Unit (1977)

$$St = E Re^{-0.205} Pr^{-0.505}$$

$$E = 0.0225 \exp(-0.0225(\ln Pr)^2)$$

Where

- *St* = Stanton number
- $h_i$  = fluid film coefficient,  $W/m^2 C$
- $\rho$  = fluid density,  $kg m^{-3}$
- $C_p$  = fluid specific heat capacity,  $J/kg C$
- *Re* = Reynolds number (ratio of momentum to viscous forces)

- $Pr$  = Prandtl number (ratio of momentum diffusivity to thermal diffusivity)
- $Nu$  = Nusselt number (ratio of convective to conductive heat transfer)

This equation is applicable for flows with Reynolds number greater than 10000.

## 6 Mechanical Design

Below are described mechanical aspect of the project, such as heat exchanger and pump design, as well as pipe material selection, and pipe thickness that's required to withstand the pressures and temperatures experienced in the system.

### 6.1 Heat Exchanger Design

After the depth of 1000 m is achieved the fluid under the force of pressure has become quite dense, as can be seen from the figure from the previous chapter, the density increased by nearly  $500 \text{ kg m}^{-3}$ .

At this point the fluid enters the heat exchanger. On the outside of the heat exchanger hot geothermal water rises from the ground at around  $90 \text{ C}$ , at a rate of  $200 \text{ m}^3 \text{ h}^{-1}$ .

Because of the limited space inside of the geothermal well, the design of the heat exchanger was chosen to be a 2 tube pass 1 shell pass heat exchanger, which would look like the one in figure 6.1.1:

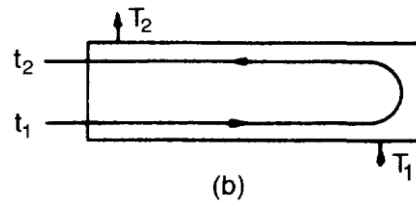


Figure 6.1.1

For a heat exchanger, the design equation is the following:

$$Q = UA\Delta T_m$$

Where

- $Q$  – Heat Transferred Per Unit Time (W)
- $U$  – Overall Heat Transfer Coefficient,  $\text{W/m}^2 \text{ } ^\circ\text{C}$
- $A$  - Heat Transfer Area,  $\text{m}^2$
- $\Delta T_m$  – True Temperature Difference,  $^\circ\text{C}$

The overall Heat Transfer Coefficient (39) can be determined with the following equation:

$$U = \frac{1}{\frac{1}{h_o} + \frac{d_o - i_{ns} \ln\left(\frac{d_o - i_{ns}}{d_i - i_{ns}}\right)}{2k_{ins}} + \frac{d_o \ln\left(\frac{d_o}{d_i}\right)}{2k_w} + \frac{d_o}{d_i} * \frac{1}{h_i}}$$

Where

- $h_o$  – Outside fluid film coefficient,  $W/m^2 C$  ( $\lambda_o$ )
- $h_i$  – Inside fluid film coefficient,  $W/m^2 C$  ( $\lambda_i$ )
- $k_w$  - Thermal conductivity of the tube wall material,  $W/m^2 C$
- $d_i$  - Inside tube diameter, m
- $d_o$  - Outside tube diameter, m
- $d_{o-ins}$  – Insulating material outside diameter, m
- $d_{i-ins}$  – Insulating material inside diameter, m
- $k_{ins}$  – insulating material thermal conductivity  $W/m^2 C$

For the determination of the True temperature difference, the 1<sup>st</sup> thing required to do is to determine the LMTD (39) (Log Mean Temperature Difference)

$$\Delta T_{lmtd} = \frac{(T_1 - t_2) - (T_2 - t_1)}{\ln \left( \frac{T_1 - t_2}{T_2 - t_1} \right)}$$

Because the flow here is a mixture of co- and countercurrent flow, a correction factor is required,  $F_t$ .

The true temperature difference is therefore given by  $\Delta T_m = F_t \Delta T_{lm}$

The correction factor (39) is a function of the shell and tube fluid temperatures, and the number of tube and shell passes. It is normally correlated as a function of two dimensionless temperature ratios:

$$R = \frac{T_1 - T_2}{t_2 - t_1}$$

$$S = \frac{t_2 - t_1}{T_1 - t_1}$$

**R** is equal to the shell side fluid flowrate times the fluid mean specific heat, divided by the tube side fluid flowrate times the tube side fluid specific heat.

**S** is a measure of the temperature efficiency of the exchanger.

For 1 shell 2 tube pass exchanger, the correction factor (39) is:

$$F_t = \frac{\sqrt{(R^2 + 1)} \ln \left( \frac{1 - S}{1 - RS} \right)}{(R - 1) \ln \left( \frac{2 - S \left[ R + 1 - \sqrt{(R^2 + 1)} \right]}{2 - S \left[ R + 1 + \sqrt{(R^2 + 1)} \right]} \right)}$$

## 6.2 Material for construction

Different materials have been considered for the piping used in the system. The most important economic aspects that played the role in selecting the metal for the task were the cost, thermal conductivity, and pipe thickness (yield stress related). The results are displayed in the following table:

Material	Length of HX, m	Cost per ton, USD	Design Stress, MPa	Thermal Conductivity, W (m K) <sup>-1</sup>	Cost, USD	Thickness, m
Aluminum	5	2500	260	205	6470.012	0.003
Stainless steel (304)	44	1500	215	16	15711.66	0.004
Silver	3	498340	83	406	17261206	0.01
Copper	3	6500	70	385	253568.3	0.013
Titanium	38	55000	1480	19	79587.54	0.001
1090 Steel	15	825	540	50	4138.564	0.002

Table 6.4.1

From table 6.4.1 is seen that from all of the materials the best option is constructing the system out of 1090 Steel. This material is superior in all perspectives – it's the cheapest construction material, the design stress is also large enough to provide a small wall thickness (2 mm), and the resulting length of the bottom heat exchanger is acceptable in length. Therefore it is recommended as the construction material of choice.

One more aspect that needs to be considered when designing the system is temperature considerations. Aluminium has a tendency to soften at elevated temperatures, and it has to be taken into account at temperatures above 100 C. Since the system is operating at 90 C, which is quite close to 100 C, due to safety considerations the pipe wall thickness should be increased, which will decrease the heat transfer rate. Steel however is a lot more stable at high temperatures, which is also why it is recommended to be used as the construction material of choice.

### 6.3 Positive Displacement Pump

The positive displacement pump was chosen for this system as a method of energy extraction. The reason for such a decision is because the working fluid has a very low viscosity, and therefore a large portion of it will not hit the turbine fans, but actually leak through the system without doing any useful work. The assumption for this process is that the system is isenthalpic, i.e. the enthalpy in the system remains constant, and there's not heat exchange happening with the surroundings.

$$-W = \frac{1}{\gamma - 1} P_1 \dot{V}_1 \left[ \left( \frac{P_2}{P_1} \right)^{\frac{\gamma-1}{\gamma}} - 1 \right]$$

$$\frac{T_2}{T_1} = \left( \frac{P_2}{P_1} \right)^{\frac{\gamma-1}{\gamma}}$$

Where  $\gamma = \frac{c_p}{c_v} = \frac{c_p}{c_p - R}$ .

Since the heat capacity of supercritical CO<sub>2</sub> is strongly dependent on both temperature and pressure, no simple correlations have been developed to accurately predict the heat capacity of the fluid. Therefore, a software called Fluidprop has been utilized in the algorithm to give accurate heat capacity data.

## 6.4 Wall thickness calculation

The wall thickness for pipes was calculated from an equation used for calculating shell thickness for cylindrical vessels. For safety reasons the design pressure was taken 10 % above the maximum operating pressure in the system (13.7 MPa at the bottom of the column). The design pressure in this case will be 15 MPa. The formulae for calculating the shell thickness is following (39):

$$e = \frac{P_i D_i}{2f - P_i}$$

Where:

- $P_i$  – internal pressure (N mm<sup>-2</sup>)
- $D_i$  – inside pipe diameter (mm)
- $f$  – design stress (N mm<sup>-2</sup>)

## 7 Experimental Section

An experiment has been devised to analyze the feasibility of building an actual plant. Since the performance of most equations (viscosity, thermal conductivity, and density) can easily be checked by comparing with the data provided by NIST, no experiments are necessary to check their accuracy. However, the equations that predict the behavior of the heat transfer coefficient tend to deviate from reality. This experiment has been set up to analyze the accuracy of the predictions from these equations when compared to practical results. For this purpose a mathematical computational software Matlab has been used.

### 7.1 Development of the experimental apparatus

The experimental apparatus (figure 7.1.1) for this experiment consists of two single tube heat exchangers. Since the pump used in this experiment is only capable of pumping liquid CO<sub>2</sub>, the role of the 1<sup>st</sup> heat exchanger will be to convert CO<sub>2</sub> from liquid to supercritical state. The 2<sup>nd</sup> heat exchanger is then used to analyze the heat transfer coefficient of the supercritical fluid, and compared with predictions done by the developed software.

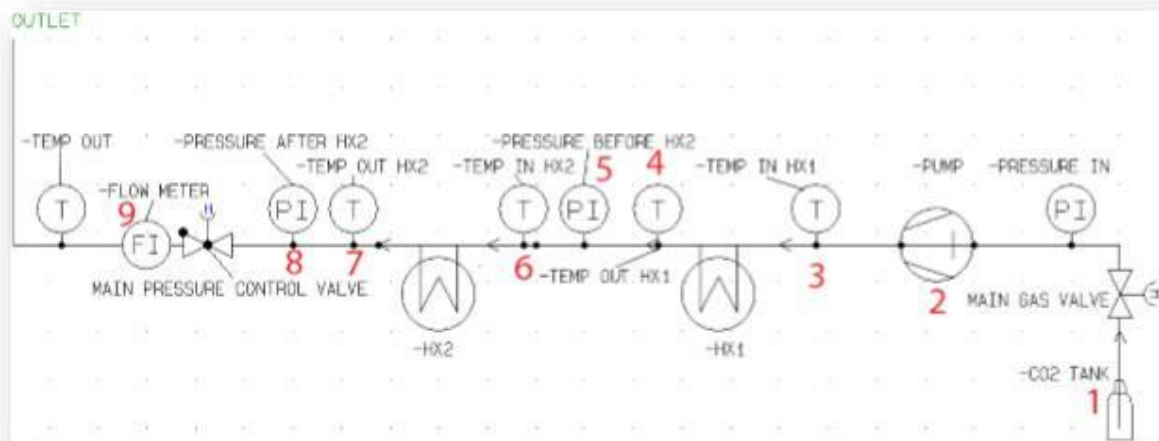


Figure 7.1.1

Liquid CO<sub>2</sub> is drawn from a contained (1) and fed to a positive displacement pump (2), where the fluid gets compressed and cooled down. After exiting the pump, the fluid flows into the 1<sup>st</sup> heat exchanger (HX1), where it experiences a transition from liquid to supercritical state. The temperature of the fluid is checked by using a thermocouple at the ends of the heat exchanger (3, 4). The pressure change of the fluid is also recorded (5) if any does occur. After that, the supercritical fluid is fed into another heat exchanger (HX2), where the fluid get heated up. Just as for the 1<sup>st</sup> heat exchanger, the temperature changes before and after are recorded (6, 7), as well as the pressure change (8). After leaving the heat exchanger the fluid goes through a control valve, which regulates the outlet pressure of the system. After the valve a flowmeter is installed to measure the volumetric flow of the gas (9). Also, a temperature probe was installed to correct use it as a correction when converting from volumetric to mass flows.

## 7.2 RMSE and errors of measurement

As any experimental data will not be exactly matched by a simulation, therefore a technique is required to take into account for errors in the system, and give predictions with certain confidence limits. This can be done by using either the standard deviation, or by using a value that's called RMSE.

RMSE – Root Mean Square Error, a technique that allows to measure the difference between a model and actually observed values. RMSR is a good measure of accuracy, but it can only forecast errors of different models only for a particular value, and can't be used for multivariate statistical analysis, as it is scale dependent.

The errors bars on the plots were generated by evaluating the uncertainty when measuring the possible temperature drop of the fluid when just exiting the heat exchanger and until it reached the measurement point (around 0.15 m distance from contact with water). The accuracy of the readings was increased when thermocouples were used, and for the case of using thermocouples inserted directly into the fluid stream, the errors of readings, and therefore predictions were minimal, less than 1 °C.

## 7.3 Parameter Verification

The model has been verified against data from openly available sources. The parameters analyzed were density, viscosity, and thermal conductivity. Everything was compared with the data available at NIST.

2 types of samples were taken – one as isobaric heating, and another is isothermal. A sample of 52 points were taken for both comparisons. The equation used in analysis to calculate the standard deviation is:

$$\sigma = \sqrt{\frac{1}{N} \sum_{i=1}^N (x_i - \mu)^2}$$

Where:

- $\mu$  - reference value (NIST)
- $x_i$  – calculated value (PR-EOS)
- $N$  – number of points taken

The standard deviation for density was found to be  $\pm 28.85 \text{ kg m}^{-3}$ . The results were plotted in isobaric and isothermal plot comparison.

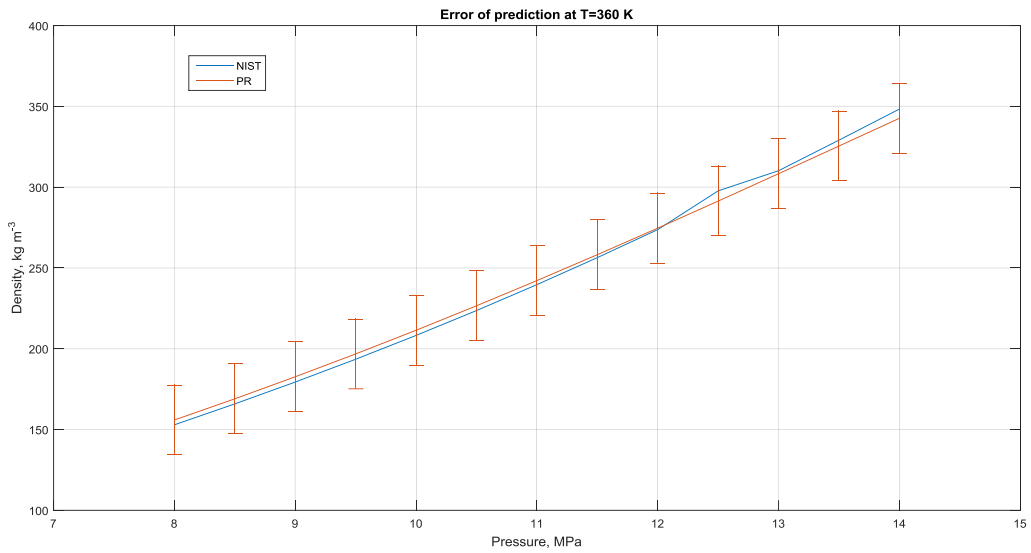


Figure 7.3.1

As seen in the isothermal plot (figure 7.3.1), the values predicted by PR-EOS match quite closely to data provided by NIST, and the standard deviation fits very well with the predicted density.

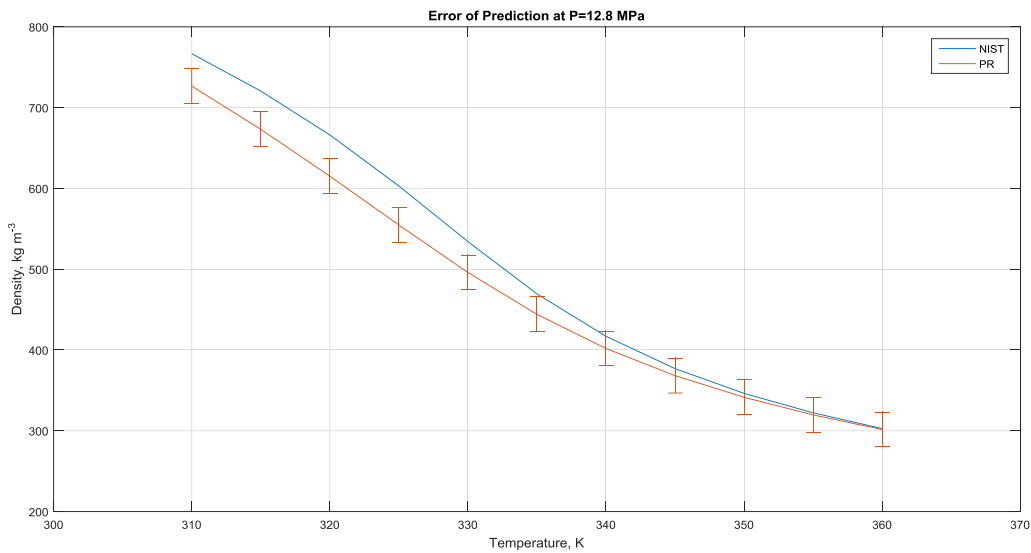


Figure 7.3.2

On the isobaric plot (figure 7.3.2) it is seen however, that the PR-EOS appears to undershoot with its predictions on fluid density, at certain points deviating even more than the standard deviation predicts. However it is seen that at high temperatures the results of the PR-EOS match the data provided by NIST quite closely.

The equation that predict additional fluid properties such as thermal conductivity and viscosity is said to give an average absolute deviation of about 4% for viscosity predictions and 6% for thermal conductivity, which means that the model is satisfactory for engineering purposes.

Although reliable equations have been developed to predict fluid viscosity, density and conductivity, a problem arises when considering heat transfer. To analyze the performance of the heat transfer equations, an experiment has been set up to analyze the performance of a set of equations.

#### 7.4 Experimental Procedure

A number of experiments were run at different pressures, starting from subcritical 7 MPa, and with a step of 1 MPa increasing the operating pressure up to 20 MPa. The heat exchanger was submerged in a stirred tank filled with boiling water, and boiling was maintained throughout the experiment. A gauge was mounted after each heat exchanger to monitor the pressure drop after the fluid left the heat exchanger, and temperature sensors were recording the temperature difference of the walls of the heat exchanger at both ends. A crude flow estimator was mounted at the end of the system to measure the approximate volumetric flowrate. A thermometer was mounted on the exhaust of the flowmeter to measure the gas temperature, which would later be used for any corrections when calculating the volumetric flow of the gas.

#### 7.5 Development of the algorithm

Since the program will be predicting practical results, it has to be modelled based on a physical system. The system that has been used in this experiment is based on a tube heat exchanger (stainless steel). The length of the heat exchanger has been selected to be 1 m long, with an ID of 2 mm, and an OD of 3.175 mm (1/8"). This pipe was selected due to its ability to sustain pressures of up to 40 MPa without risk of rupture. Such a length of the heat exchanger has been selected for convenience purposes, although the developed program is flexible enough to allow different dimensions to be applied for calculations.

Although initially the length of the heat exchanger was meant to be 1m exactly, due to difficulties during construction of the heat exchanger the length had to be increased up to 1.2m. This was not an issue though, since the algorithm developed took this extra length into consideration.

An assumption was made that the heating fluid stays at constant temperature,  $T_w = 100$  °C. This temperature was selected for convenience purposes, since it is easier to maintain a water tank at boiling temperature instead of a sub-boiling temperature. It was also assumed that on small enough distances fluid properties behave in a linear manner. For this simulation a step size of 1 cm has been selected, which meant the program would have to run 100 times to give an end result.

The program starts predicting fluid properties (density, viscosity, thermal conductivity, and velocity) based on given inside diameter, temperature and pressure. Based on that information the Heat Transfer Coefficient is calculated. Based on the difference of the fluid and water temperature, the LMTD is calculated. Using the equation  $Q = U * A * T_{LMTD} * \frac{l}{u}$ , the amount of heat transferred to the CO<sub>2</sub> is calculated. Since the energy in the original form of the equation is given in W (J s<sup>-1</sup>), an adjustment factor was required  $\frac{l}{u}$  (s), which accounts for the residence time of the fluid within the test segment. Knowing the amount of heat that is transferred, a temperature change can be calculated by  $T_{new} = \frac{Q}{C_p * \dot{m}} + T_{old}$ , where  $\frac{Q}{C_p * \dot{m}}$  is the  $\Delta T$ , or the temperature rise of fluid in the control volume. After, the pressure losses are

calculated. Coulson and Richardson (1999) suggests to use  $8f$ , where  $f$  is the Darcy friction factor. An adjustment is then made to the pressure by  $P_{new} = P_{old} - \Delta P$ . This finishes the calculations, and a new loop is started with the updated values of temperature and pressure.

## 7.6 Results

The heat exchangers were run multiple times, with a starting pressure of 7 MPa, and with a step on 1 MPa increased until 20 MPa in the 1<sup>st</sup> run, and 22 MPa in all the rest of the experiments. Throughout the experiment the heating medium (water) was maintained at boiling temperature, with the biggest possible drop in temperature of 2 °C. The 2 runs are presented in different graphs. Both however were run with slightly varying the mass flowrate, since for the experiment only 1 pressure release valve was used, which often got blocked because of deposition of ice due to cooling at near adiabatic conditions while expanding out of the pressurized heat exchanger and into ambient environment.

1<sup>st</sup> set:

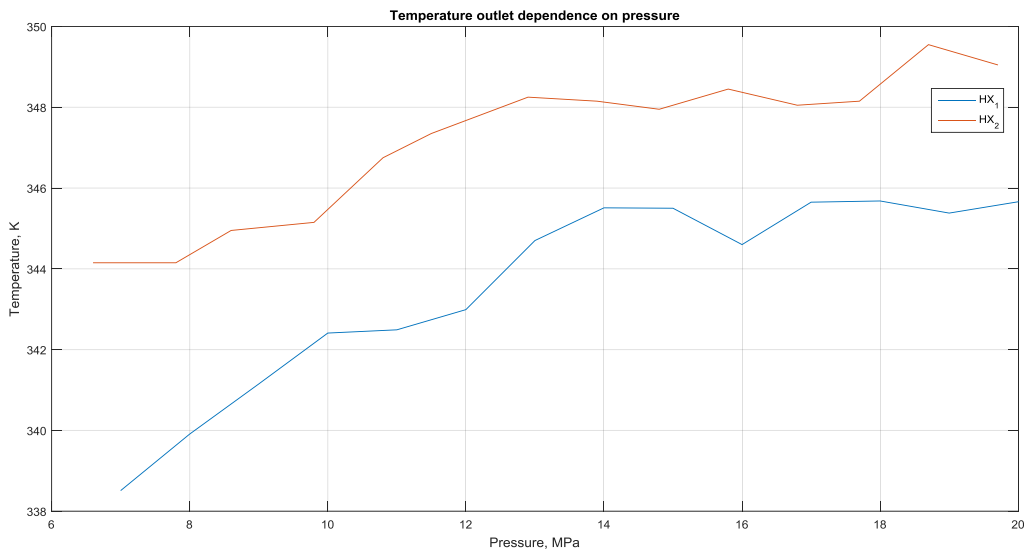


Figure 7.6.1

As seen in figure 7.6.1, at lower pressures (up to about 14 MPa) a significant increase in HX outlet temperature is observed, which is attributed to increasing density of the fluid in the system. However, about 14-15 MPa it is observed that the outlet temperature appears to be reaching a stable value, with no significant increase in fluid temperature as the pressure is increased.

2<sup>nd</sup> set:

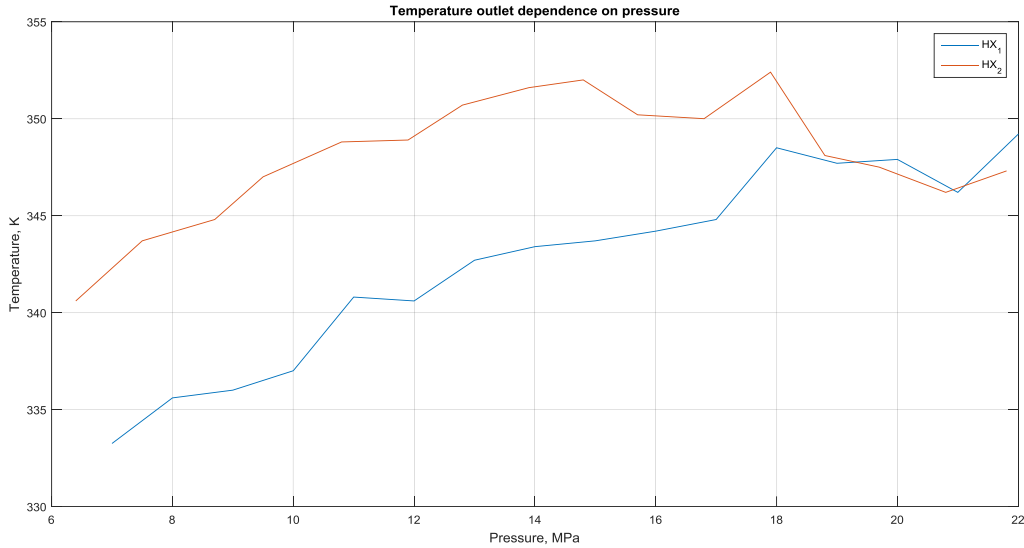


Figure 7.6.2

The 2<sup>nd</sup> experiment (figure 7.6.2) was also run with boiling water as the heating medium, though slightly different mass flowrate was chosen, due to the pumps inability to stabilize the pressure. The trend of heat transfer however is also observed in this set, as it was in the previous one. The outlet temperature appears to stop increasing after around 14-15 MPa, and for the 2<sup>nd</sup> HX it appears to even drop.

## 7.7 Analysis

The experimental data was used to check the applicability of a number of heat transfer equations, most of which revolve around Nusselt number, and one involving Stanton number. Plots were generated displaying the real fluid temperature out of the heat exchangers, and the temperatures predicted by the heat exchanger algorithm.

Premature calculations based on the mass flow through the system showed that all flows were either transitional or turbulent at the inlet in the 1<sup>st</sup> heat exchanger.

### 7.7.1 Petukhov-Kirillov

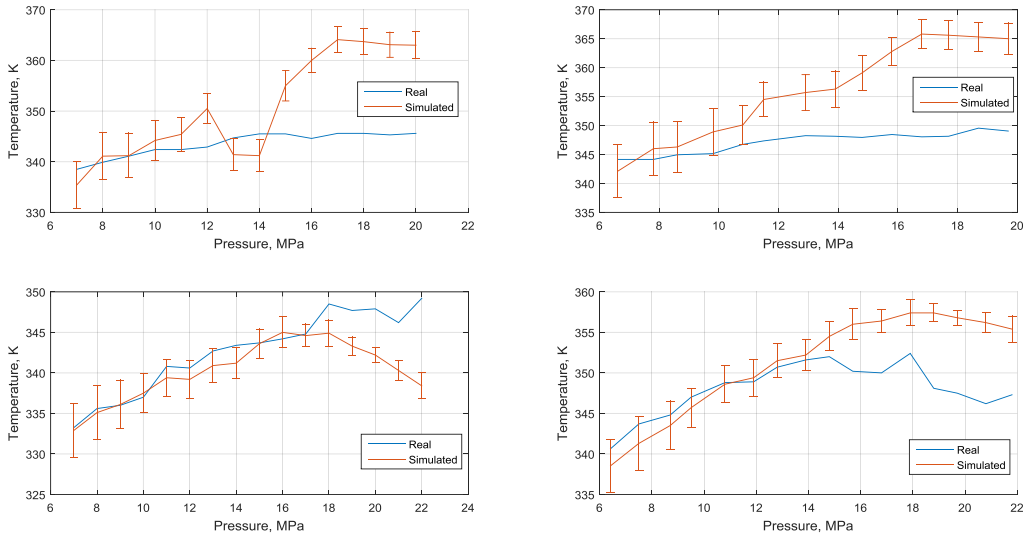


Figure 7.7.1.1

As seen from in the graphs (figure 7.7.1.1), the simulated data fits quite well with the experiments, but this behavior tends to diverge at higher pressures. The RMSE of the prediction against the experimental results has been calculated to be 7.8 °C. However the high pressure calculations were only made for experimenting interest, and the highest pressure achievable in a full scale hydrothermal plant would be only 15-16 MPa. The RMSE for prediction in this case is only 3.5 °C, which makes it a fairly accurate equation to use for predicting the Heat Transfer Coefficient.

### 7.7.2 Gnielinski correlation

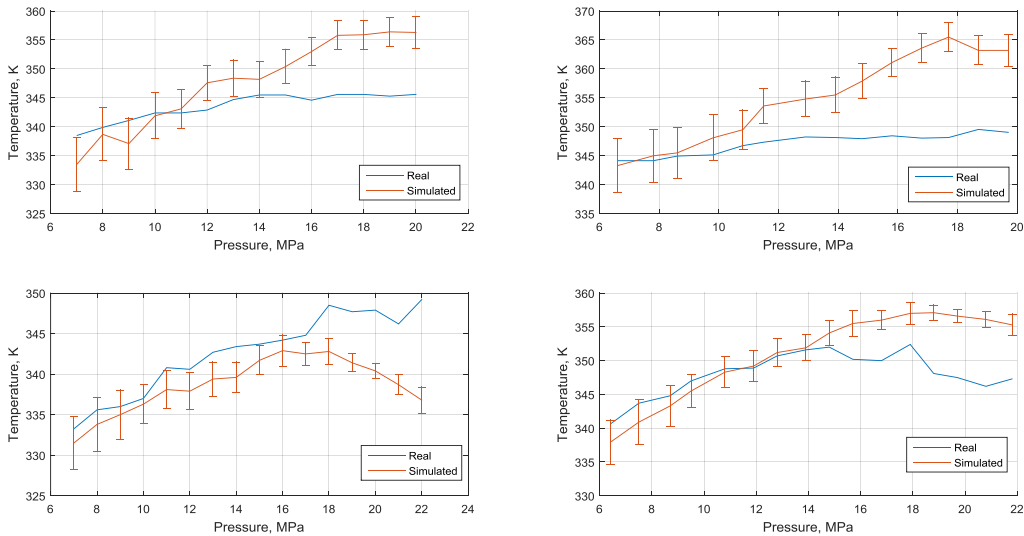


Figure 7.7.2.1

This correlation is a modification of the original Petukhov-Kirillov (P&K) equation that extends its applicability into the transitional flow regime. As seen on the plots (figure 7.7.2.1), the predicted data fits experimental results even better than the (P&K) correlation. That is clearly demonstrated when the RMSE

is considered: 6.6°C for the full range of pressures, and 3.2°C for pressure range of up to 16 MPa. The effectiveness of this equation can be attributed to its applicability in the transitional flow regime. Even though  $Re$  for the flows is above 2000, it doesn't go over 10000, suggesting there might be transitional flows occurring somewhere in the system. Also the equation seem to be more stable than P&K correlation, i.e. it doesn't seem to display high deviations from the trend, as it is seen in the 1<sup>st</sup> plot of the P&K simulation.

### 7.7.3 Dittus-Boelter

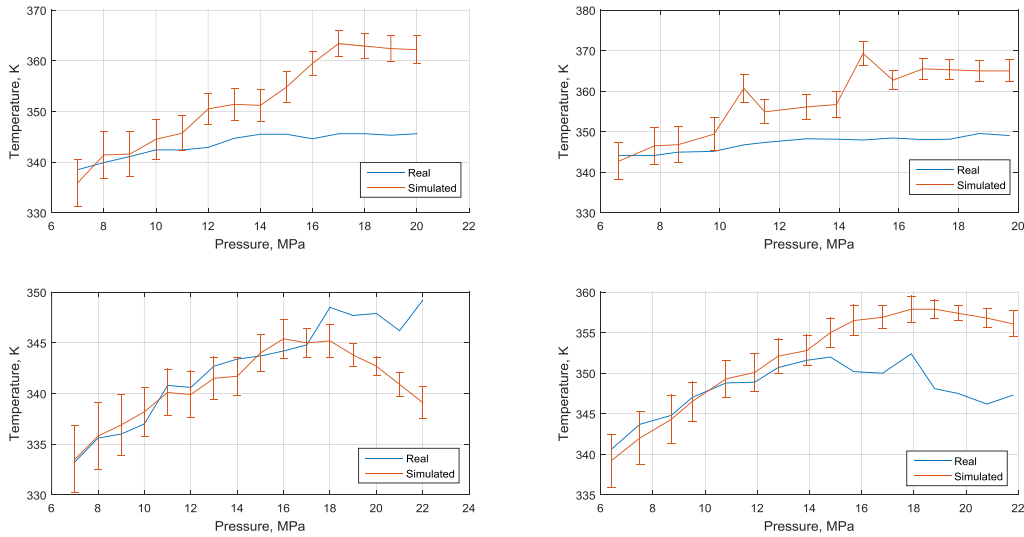


Figure 7.7.3.1

3<sup>rd</sup> equation considered is from Dittus-Boelter (1930), and although it is one of the simplest Heat Transfer equations that were developed, it predicts the heat transfer quite well (figure 7.7.3.1), with the RMSE even better than Petukhov-Kirillov correlation - 7.7°C for full range of pressures and 3.5°C for pressures up to 16 MPa.

## 7.7.4 ESDU

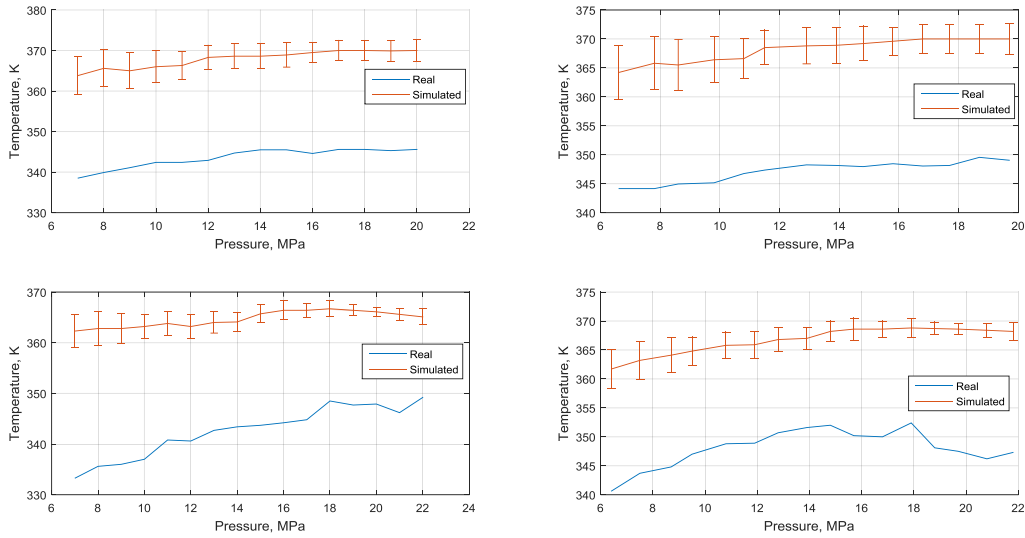


Figure 7.7.4.1

As seen from the plots (figure 7.7.4.1), this equation gives an overestimation of the fluid outlet temperature, and thus can't be considered to be used in any simulations.

## 7.7.5 Schwarz

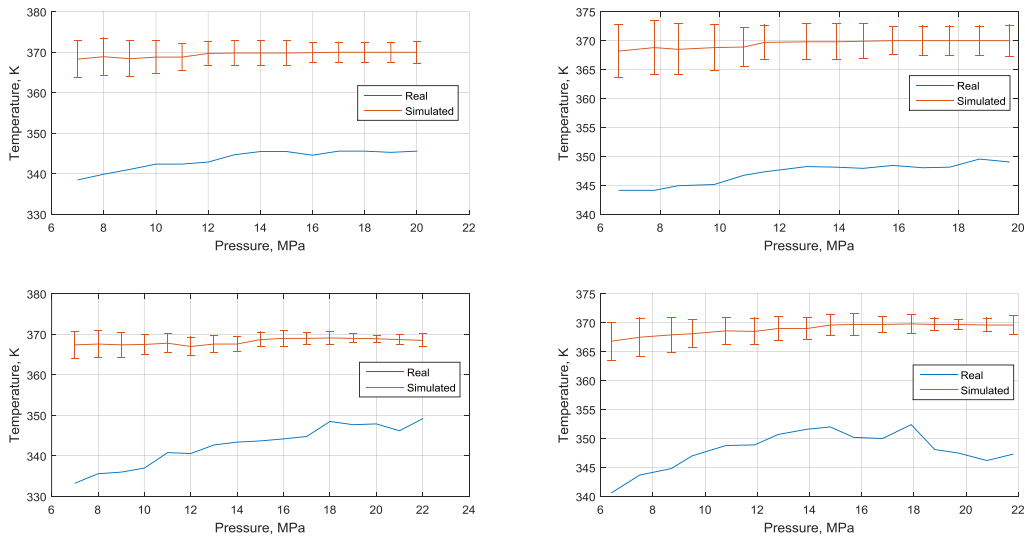


Figure 7.7.5.1

As seen in figure 7.7.5.1, Schwarz correlation performs similarly to the ESDU correlation and overestimate the heat transfer coefficient, giving rise to huge errors when estimating the fluid outlet temperature.

## 7.8 Additional experiments

Since some experimental data appeared to deviate severely from simulation data, another set of experiments has been performed to confirm or disprove if the deviation really does occur at high

pressures. For this reason a 16 runs at different pressures has been performed (7-22 MPa, with a step of 1 MPa), with the CO<sub>2</sub> passing through the heat exchangers that were submerged in boiling water. This setup utilized only thermocouples attached to the walls of the heat exchangers for temperature reading. It was noticed that the thermocouple readings differed from liquid thermometer readings in some places by around 5 °C, which significantly improved accuracy of readings.

### 7.8.1 Experimental Results

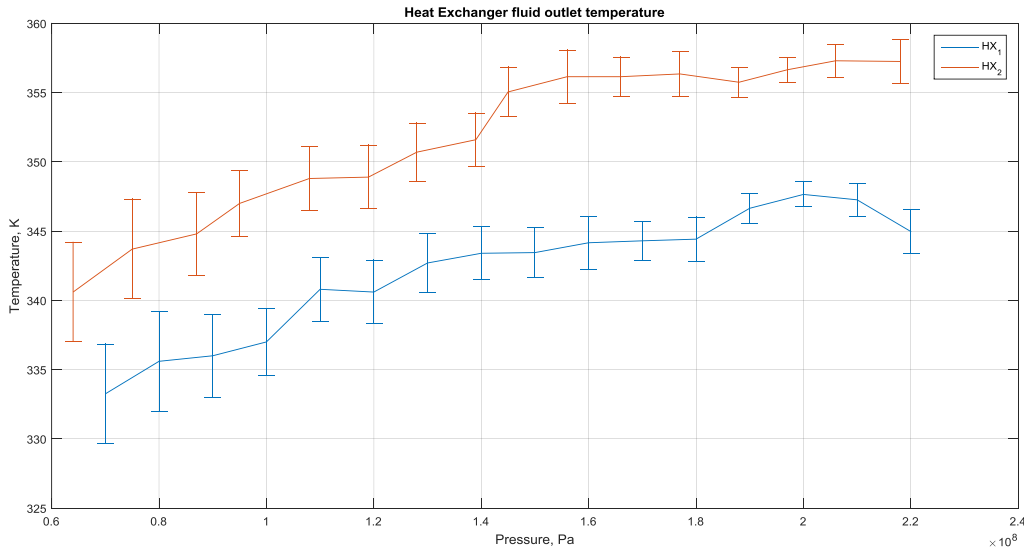


Figure 7.8.1.1

The additional experiments indeed show a more expected behavior (figure 7.8.1.1), with practically no drop in heat transfer with increased pressure. Also, as expected the rate of heat transfer slows down as higher pressure are reached. The conclusion with the experimental section is that this data set is a reliable representation of what actually happens with the fluid inside of the Heat Exchangers. The further sections will apply the information obtained from experiments and apply them to the simulation, to compare how the predictions perform against experimental data.

## 7.8.2 Petukhov-Kirillov

### 7.8.2.1 HX<sub>1</sub>

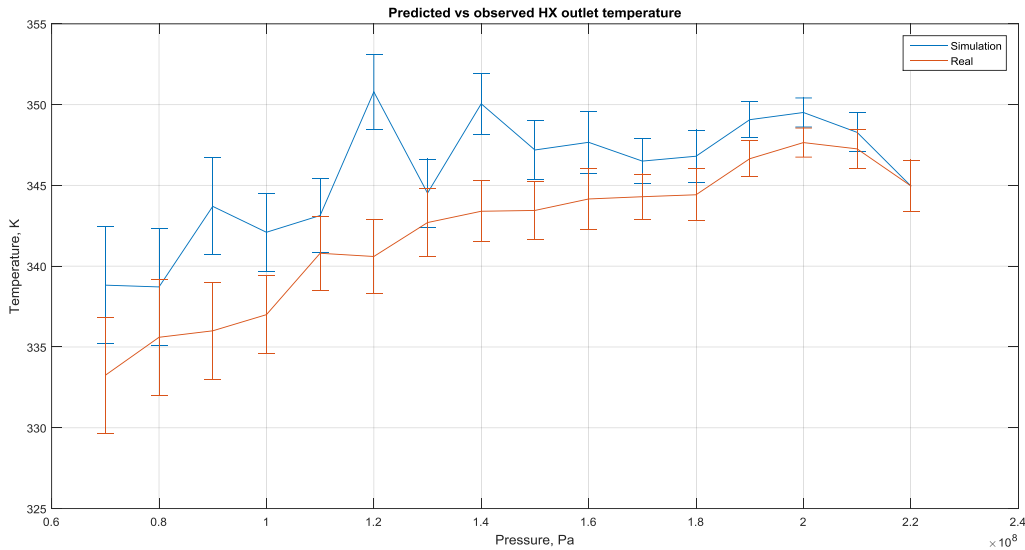


Figure 7.8.2.1.1

Analysis on the 1<sup>st</sup> HX using the Petukhov-Kirillov correlation (figure 7.8.2.1.1) shows that there is actually more deviation appearing at the lower pressure region that it does on the high pressures. Also, it has been noted that there are some instabilities in the algorithm that produce deviations in temperature predictions, which can be seen at 12 and 14 MPa. A problem that the algorithm can encounter during the calculations is that there is a phase transition of CO<sub>2</sub> in the HX from liquid to supercritical, and as stated in the description of the EOS, it gives 'reasonably accurate' predictions of fluid behavior in that region. Therefore for that region of the HX, only 'reasonably accurate' results are obtained, which can play a key factor in the errors that the algorithm gives when predicting the outlet temperature. However overall the performance of the correlation is evaluated as positive, with an RMSE of 4.5 °C.

### 7.8.2.2 $HX_2$

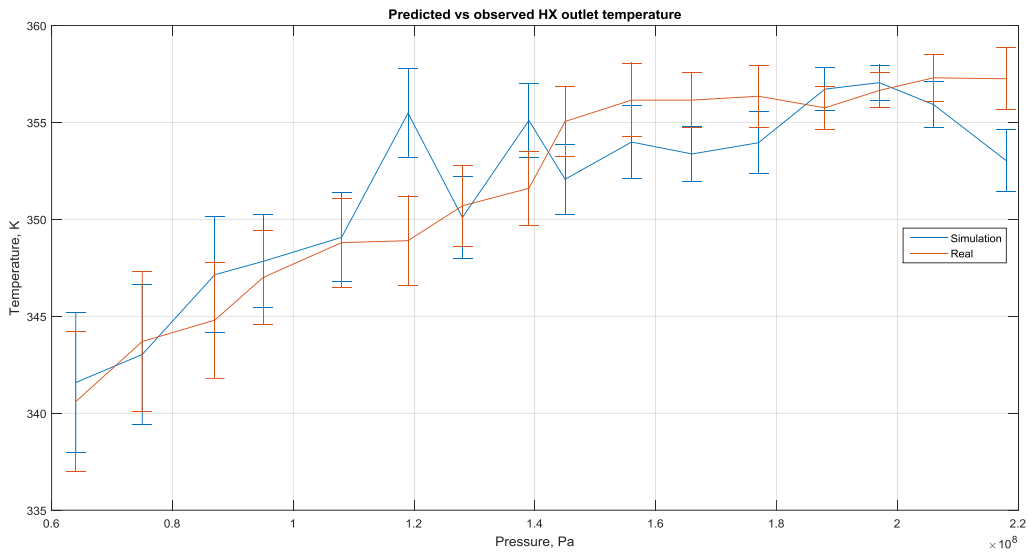


Figure 7.8.2.2.1

The correlation appears to perform better when the fluid is fully supercritical, and this also can be attributed to the fact that the fluid enters the HX with a fully developed flow, and also the fluid is entirely supercritical, and there is no phase transition happening within it. On the graph (figure 7.8.2.2.1) it is seen that at some points the algorithm tends to overshoot or undershoot with the predicted values, but overall the uncertainties overlap, which is a good sign that the correlation is accurate enough to be used for simulation purposes if no other correlation performs better. The RMSE in this case is 2.6 °C.

### 7.8.3 Gnielinski

#### 7.8.3.1 $HX_1$

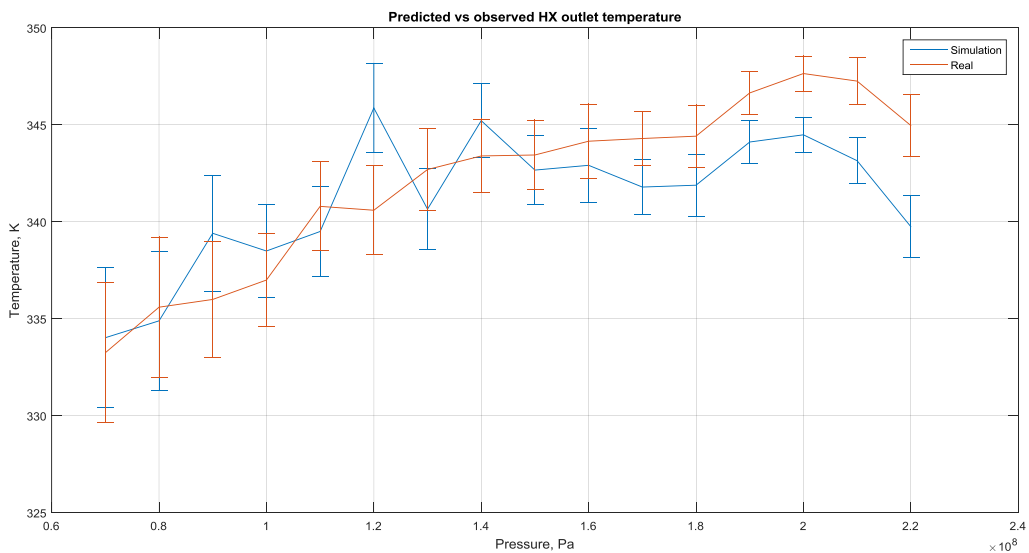


Figure 7.8.3.1.1

The next considered correlation was the Gnielinski correlation (figure 7.8.3.1.1). Too much surprise, the equation appears to be more accurate in predicting the temperatures of the fluid in the lower pressure region (up to about 15 MPa). Since this equation is a modified version of the Petukhov-Kirillov equation that is designed to extend its range of applicability into the transitional region of fluid flow, which helps with prediction of heat transfer and thus fluid behavior in general.

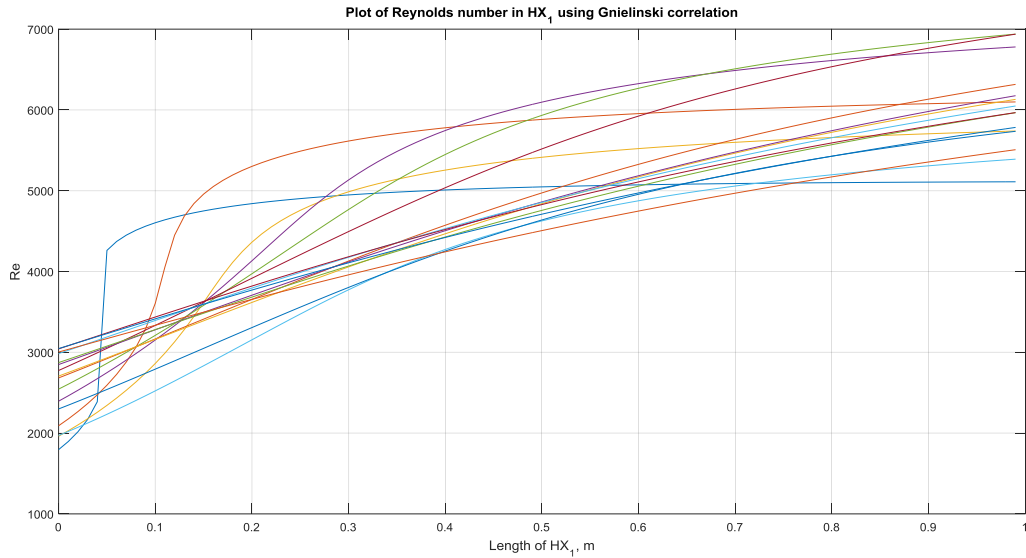


Figure 7.8.3.1.2

As seen in the Reynolds number plot (figure 7.8.3.1.2) for the HX at different temperatures, the fluid flow starts in the laminar/transitional flow regime, and therefore Gnielinski's correlation is better suited for heat transfer predictions in that range than the Petukhov-Kirillov correlation, which is designed to deal with fully developed turbulent flow. A good representation of the accuracy with which the correlation performs is the RMSE, which is 2.8 °C in for this HX.

### 7.8.3.2 HX<sub>2</sub>

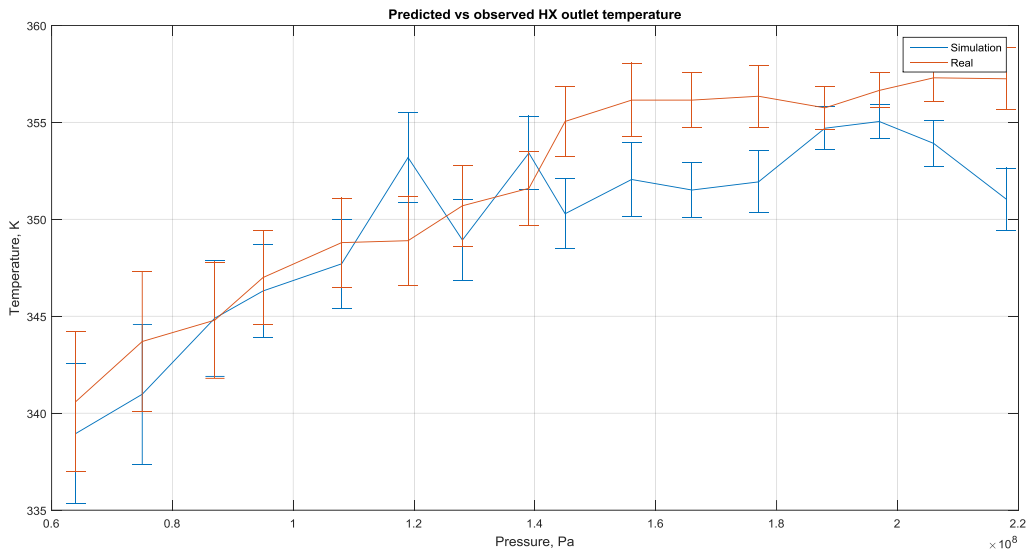


Figure 7.8.3.2.1

As with the 1<sup>st</sup> HX, the correlation appears to predict the temperatures in the lower pressure region then the higher ones. Greater deviation can be observed after about 14-15 MPa, which is consistent with the accuracy of prediction of temperatures in HX<sub>1</sub>. The RMSE in this comparison is 3.3 °C.

### 7.8.4 Dittus-Boelter

#### 7.8.4.1 HX<sub>1</sub>

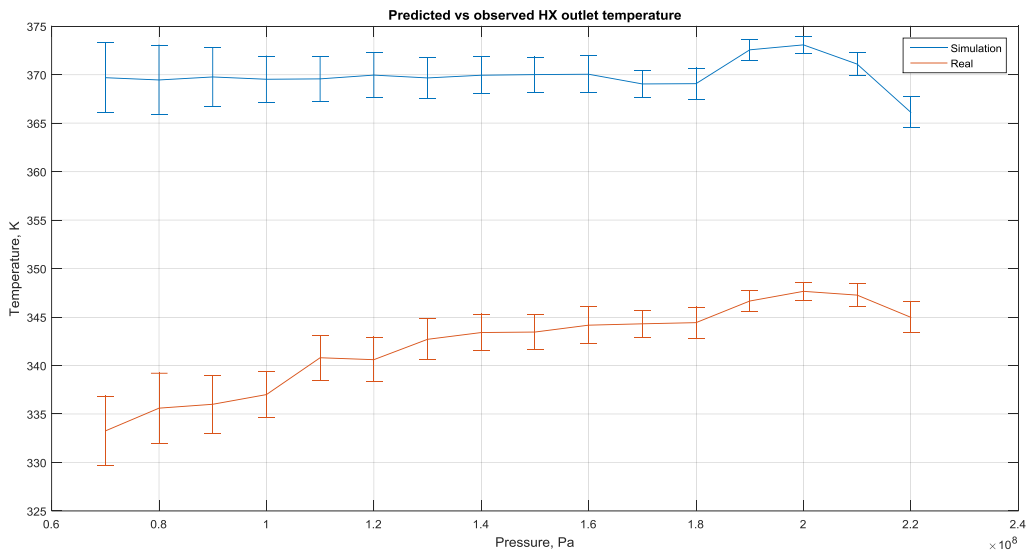


Figure 7.8.4.1.1

The next equation to be analyzed for its performance was the Dittus-Boelter, figure 7.8.4.1.1. Too much surprise the equation appears to fail to predict the heat transfer coefficient, by massively overestimating it. The RMSE in this case is 28.2, which makes it useless for making accurate simulation predictions.

### 7.8.4.2 HX<sub>2</sub>

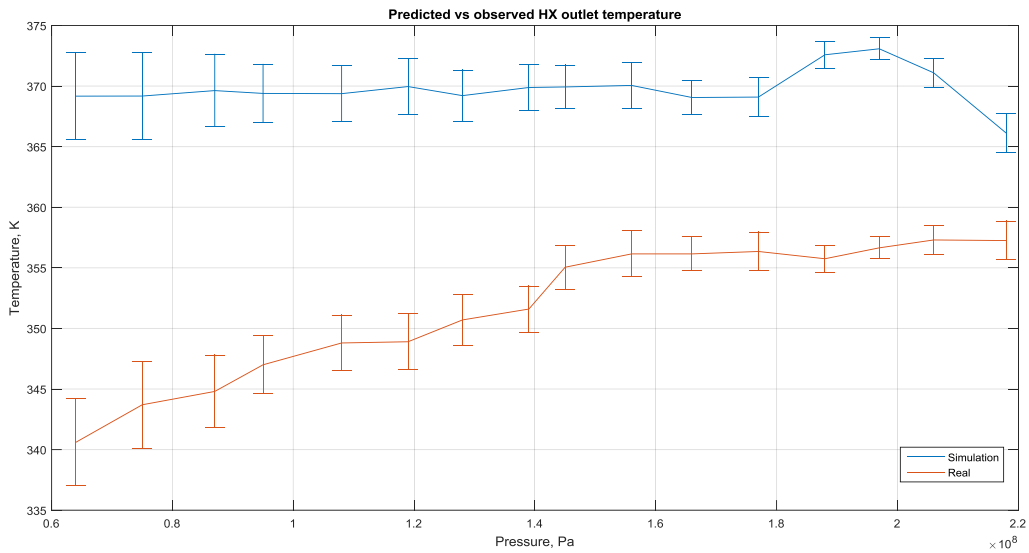


Figure 7.8.4.2.1

Much similar to the 1<sup>st</sup> HX, the equations fails to predict the heat transfer coefficient, which can be seen in figure 7.8.4.2.1, however here it does is with about 30% less error than in the 1<sup>st</sup> HX, by having an RMSE of 18.9. This also can be attributed to the fact that the equation is designed for fully turbulent flows ( $Re > 10000$ ), and the 1<sup>st</sup> heat exchanger to some extent operates in the transitional regime.

### 7.8.5 ESDU

An attempt was made to assess the performance of the ESDU equation, however the simulation fails, due to the fact that this equation overestimates the HTC by so much that the simulation reaches equilibrium, which leads to LMTD being zero, and simulation failing because of multiplying the HTC by zero.

### 7.8.6 Schwarz

The same problem has been encountered when trying to run the Schwarz correlation. The algorithm fails when LMTD drops to zero.

## 7.9 Non-dimensionless numbers

Analysis of non-dimensionless numbers was performed in order to check if the conditions to use the Heat Transfer Coefficient equations were met. Analysis has shown that the minimal Reynolds number encountered in the system was 1700, with the majority of experiments having  $Re$  between  $2 \times 10^3 < Re < 10^4$  range, and Prandtl number varying between 0.5 and 0.7, which satisfies all of the equations, apart from the Dittus-Boelter equation, which required  $Re > 10000$ .

The Nusselt number at the beginning of the HX is around 0.5-1, which afterwards shifts to around 2, which suggests that while the fluid is liquid, conduction plays a more important role in heat transfer than when the fluid transitions into a supercritical state.

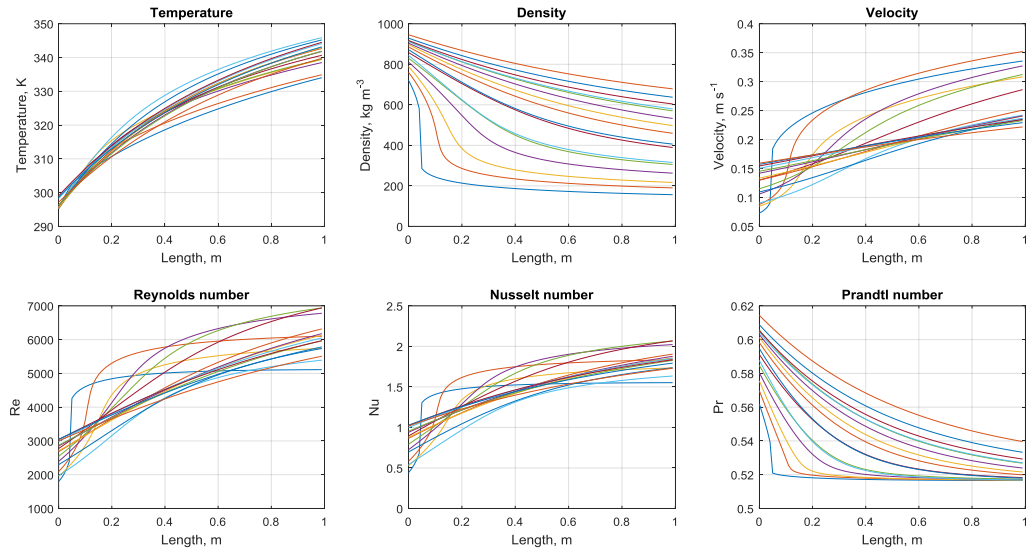


Figure 7.9.1

Figure 7.9.1 is an example of fluid behavior in the 1<sup>st</sup> heat exchanger at different pressures (7-22 MPa). An interesting fact can be observed here that the Prandtl number in all of the flows tends toward a limiting value, which is about 0.5. Since Prandtl number is lower than one, it suggests that thermal diffusivity is the dominant force in the fluid flow, and not momentum diffusivity. On the density plot it is seen how the fluid density changes with increasing pressure, and also on the very 1<sup>st</sup> line in the bottom, a clear transition is seen of a fluid going from liquid to vapor state. This blue line that corresponds to the HX operation under 7 MPa can be followed through all the plots and see how dramatically fluid properties change as the fluid undergoes this state transition. For pressures higher than 7 MPa the transitions are not so dramatic, and eventually the graphs cease to show any evident state transitions.

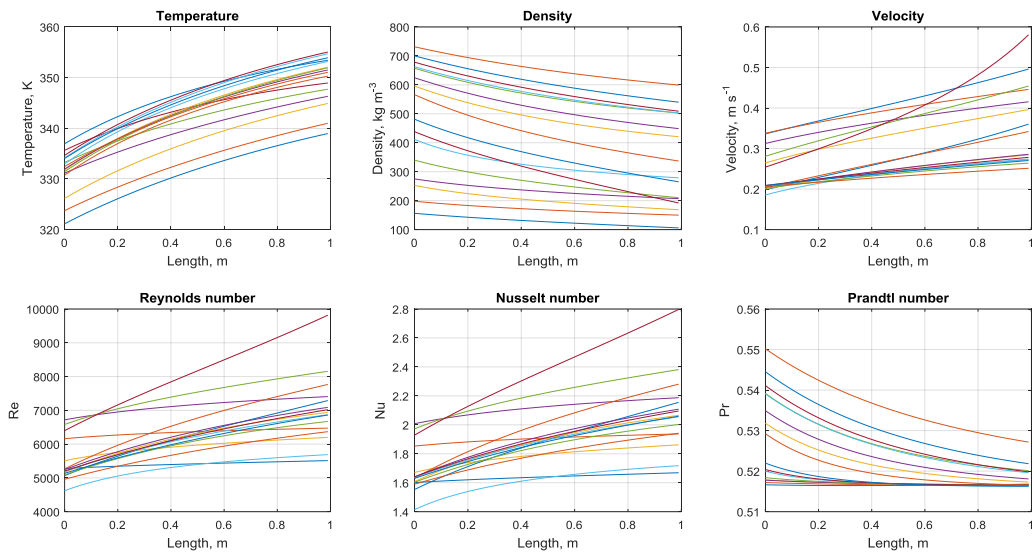


Figure 7.9.2

On the diagram of the 2<sup>nd</sup> heat exchanger (figure 7.9.2) it is observed that the values change less rapidly than they do in the 1<sup>st</sup> heat exchanger, and this is due to the fact that the  $\Delta T$  is smaller (average of 46 °C for the 1<sup>st</sup> HX versus 12 °C for the 2<sup>nd</sup> HX). Since the  $\Delta T$  is smaller, so does the LMTD decrease, which in turn decreases the amount of heat transfer, and this results in the fluid properties exhibiting a more linear behavior.

## 7.10 Extreme Temperatures

In addition to analyzing heat exchange in sub-boiling water wells, additional experiments were performed with extreme temperatures. The experiment configuration did not change, but the fluids and temperatures at which the heat exchangers operated were severely modified. The 1<sup>st</sup> heat exchanger was used to simulate heat exchange at high temperatures (180 °C), which were obtained by heating a PEG400 bath, and the 2<sup>nd</sup> heat exchanger was submerged in a water bath at 0 °C. The zero temperature was maintained by constantly adding ice into the bath, and draining excess water.

### 7.10.1 Results

#### 7.10.1.1 Heating

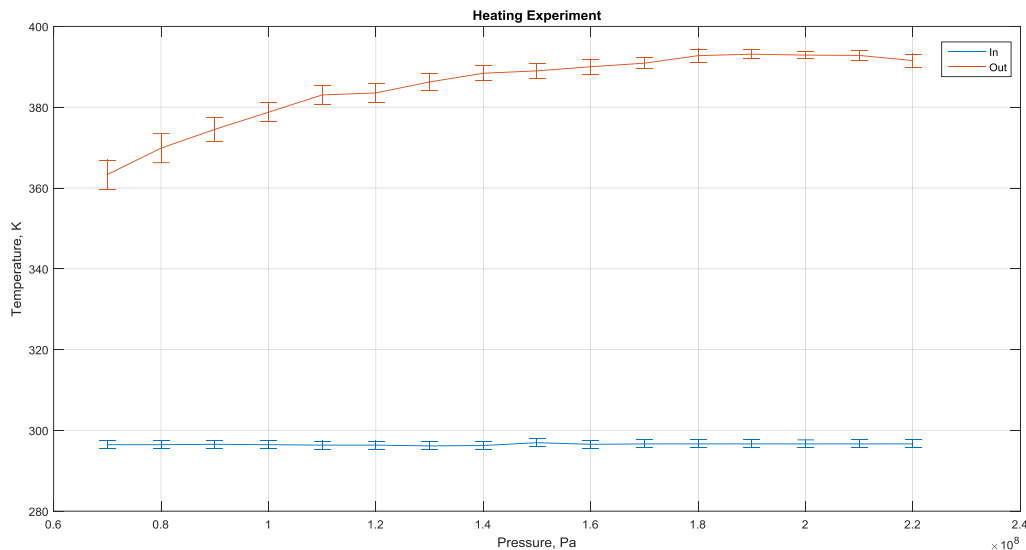


Figure 7.10.1.1.1

From experimental data it has been concluded that the CO<sub>2</sub> temperature increases with increasing pressure. This can be observed in figure 7.10.1.1.1, where the inlet temperatures and the outlet temperatures are depicted. Although the inlet temperature of the CO<sub>2</sub> remained fairly constant (varying by no more than 1 °C), it is clearly seen that the outlet temperature increases with increasing pressure. This is due to increased density of the gas, and thus higher thermal conductivity.

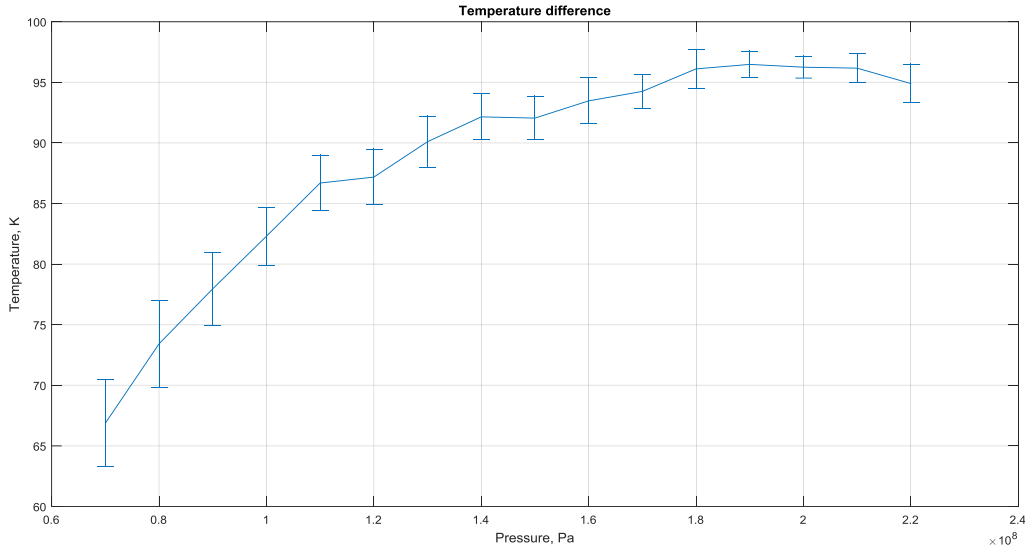


Figure 7.10.1.1.2

In figure 7.10.1.1.2 the  $\Delta T$  can be observed from the heating experiment. As seen from the plot, the temperature increase is significant with increasing pressure, reaching a maximum  $\Delta T$  of 95 °C at 18-21 MPa pressure range.

#### 7.10.1.2 Cooling

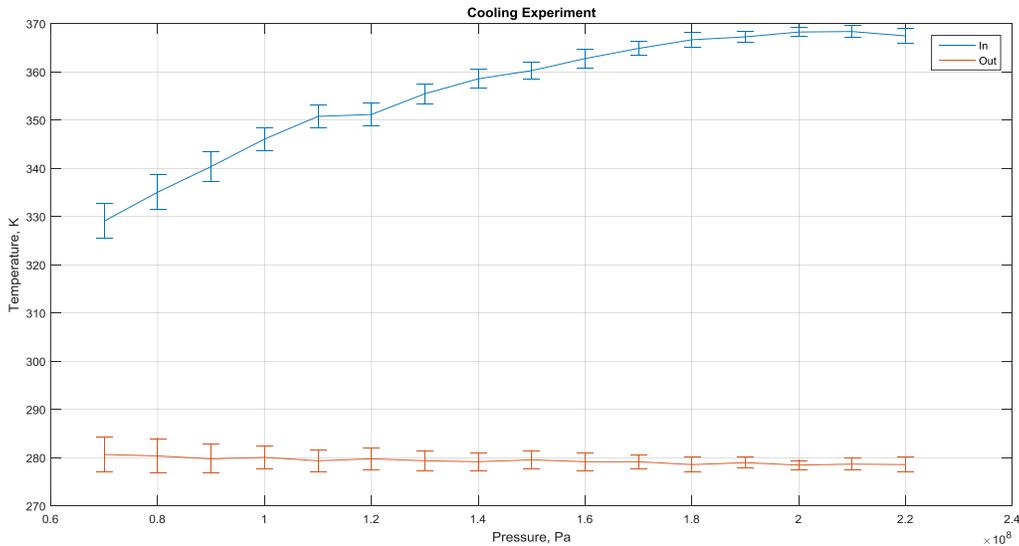


Figure 7.10.1.2.1

Since the heating and cooling were both conducted during the same experiment, the inlet temperature of the gas is increasing, much in a way that the outlet temperature increased in the 1<sup>st</sup> heat exchanger. The cooling experiment is an even more graphical representation of how a heat exchange is effected by fluid density. If looked carefully at figure 7.10.1.2.1t, it is observed that the outlet temperature of HX2 decreases, whilst the inlet temperature increases significantly. It is easier to observe this fact in the figure 7.10.1.2.2:

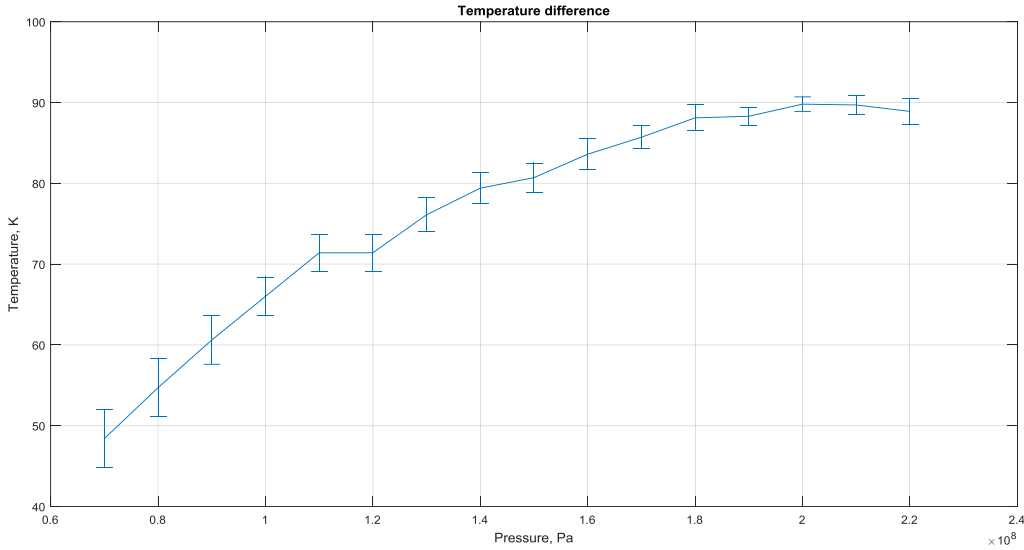


Figure 7.10.1.2.2

As seen in figure 7.10.1.2.2, at a subcritical pressure of 7 MPa, the  $\Delta T$  achieved with the 1.2m length of the heat exchanger is 'only' 49 °C, and with increase in pressure, this figure only increases, reaching up to a 90 °C at pressures or around 20-21 MPa.

## 7.10.2 Petukhov-Kirillov

### 7.10.2.1 Heating

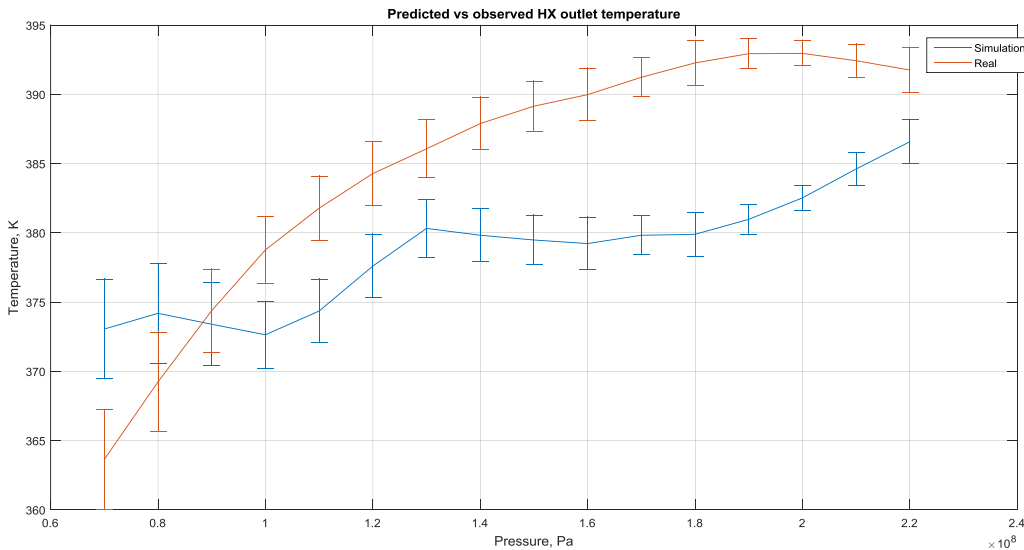


Figure 7.10.2.1.1

As seen in figure 7.10.2.1.1, the results of the simulation deviate quite significantly from experimental data, even though it is the most accurate correlation that was tested in extreme conditions. The correlation underestimates the heat transfer coefficient, and this has to be taken into account if

simulations are done. The overall RMSE for this correlation is 8.6, which is an acceptable error in simulations, and will provide acceptably accurate results.

### 7.10.2.2 Cooling

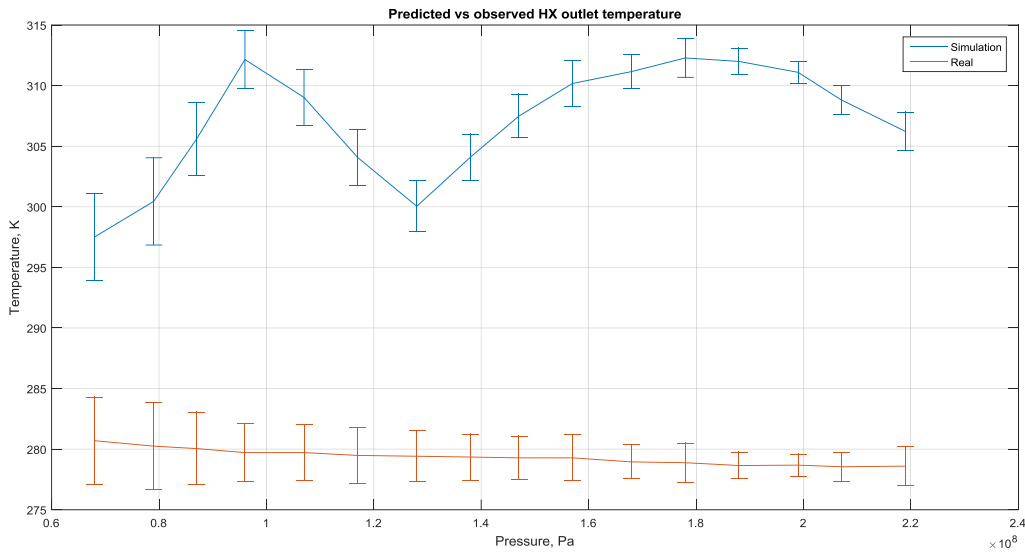


Figure 7.10.2.2.1

When the algorithm is applied to cooling CO<sub>2</sub> instead of heating, the equations fail to predict the heat transfer coefficient. As seen in figure 7.10.2.2.1, the predictions are massively overestimated and do not resemble experimental data at all. With an RMSE of 28.5 this is a very inaccurate prediction. A possible explanation is that due to the length of the heat exchanger and the amount of cooling that the fluid experiences forces the fluid to go through a state transition in the heat exchanger, which is a phenomena that is not easily modelled, and could be a key factor in contributing to the error of prediction.

### 7.10.3 Gnielinski

#### 7.10.3.1 Heating

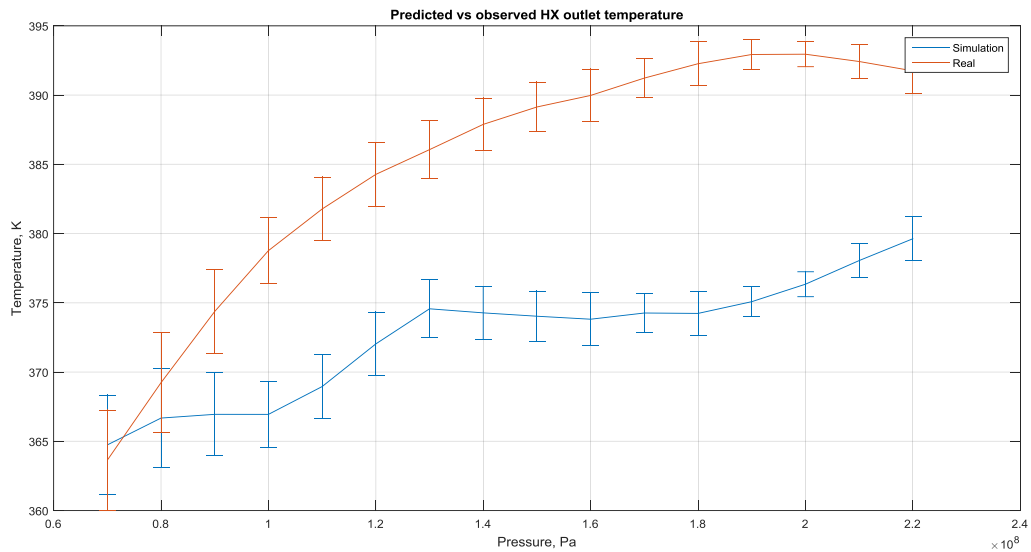


Figure 7.10.3.1.1

Even though Gnielinski's correlation outperforms Petukhov-Kirillov correlation at moderate temperatures, in the case of large temperature changes it is outperformed, which can be observed in figure 7.10.3.1.1. The RMSE in this case is 13.4, which is about 50% less accurate than Petukhov-Kirillov.

#### 7.10.3.2 Cooling

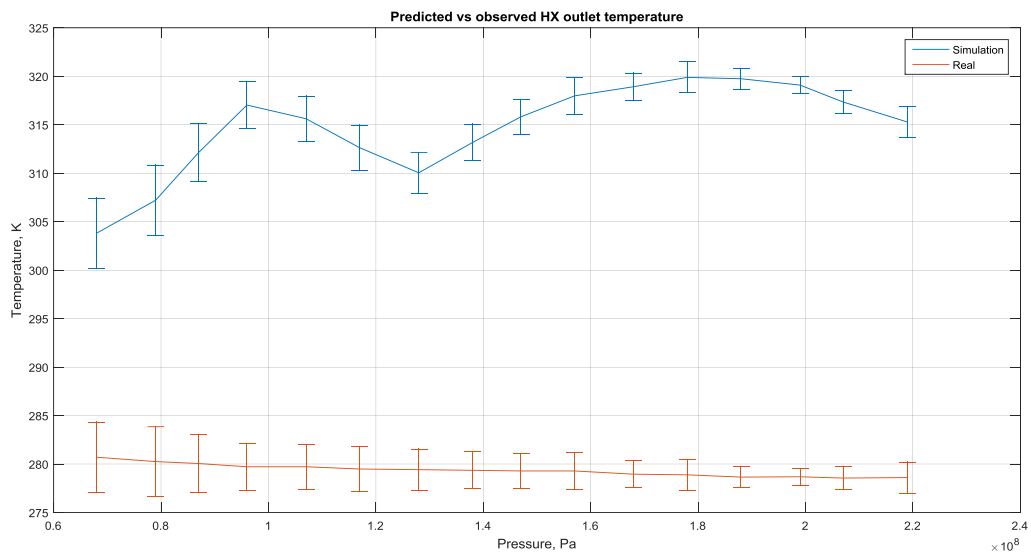


Figure 7.10.3.2.1

Similar as to the Petukhov-Kirillov correlation, the cooling predictions (figure 7.10.3.2.1) show little resemblance to what actually happens within the system. The big RMSE – 35.7 proves that for designing

cooling heat exchangers, the outlet temperatures predicted by the simulation are undershooting the heat transfer coefficient by a significant amount.

#### 7.10.4 Dittus-Boelter

##### 7.10.4.1 Heating

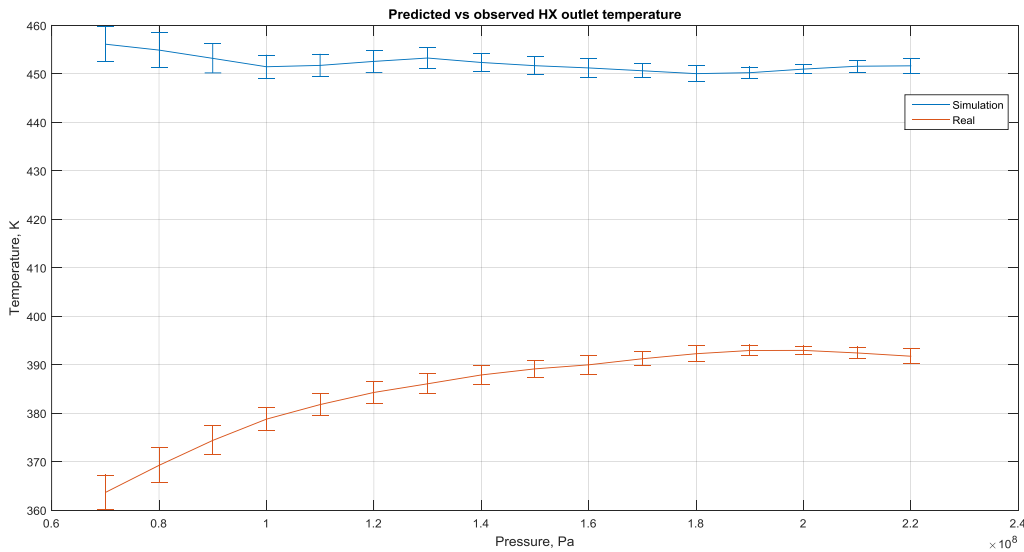


Figure 7.10.4.1.1

Although the Dittus-Boelter algorithm appears not to fail in predicting temperature of the fluid, the predictions appear to have nothing common with reality, as seen in figure 7.10.4.1.1. Also, the RMSE in this case is 68, which makes the correlation completely unreliable in predicting the heat transfer coefficient.

##### 7.10.4.2 Cooling

This equation fails to predict fluid temperature when it's subjected to cooling. This happens because the heat transfer is overestimated so much that the LMTD turns to zero, which in turn means that the heat transfer equation becomes zero, and the entire algorithm fails.

#### 7.10.5 Others

The ESDU and Schwarz correlations appear to fail to predict both heating and cooling of the fluids, by overestimating the heat transfer coefficient and leading to the failure of the algorithm.

### 7.11 Inserted Thermocouples

A suspicion was raised that measuring the fluid temperature through the HX wall will cause significant errors in readings, therefore effort was made to fix this problem. The solution was to insert the thermocouples directly into the fluid stream. This was done with the use of a pair of T junctions before and after the heat exchanger. Pressure gauges were also located before and after the heat exchanger to measure the occurring pressure drop in the system. Also, another modification was made to the 2<sup>nd</sup> heat exchanger (the fully supercritical one), by increasing the length of the heat exchanger. This was done to test the pressure drop change with increasing length of the heat exchanger. Additionally, additional thermodynamic software was merged with Matlab, called FluidProp, to aid in predicting fluid Heat Capacity. This makes this experimental set, and the simulation results the most accurate.

## 7.11.1 Results

### 7.11.1.1 1<sup>st</sup> Heat Exchanger

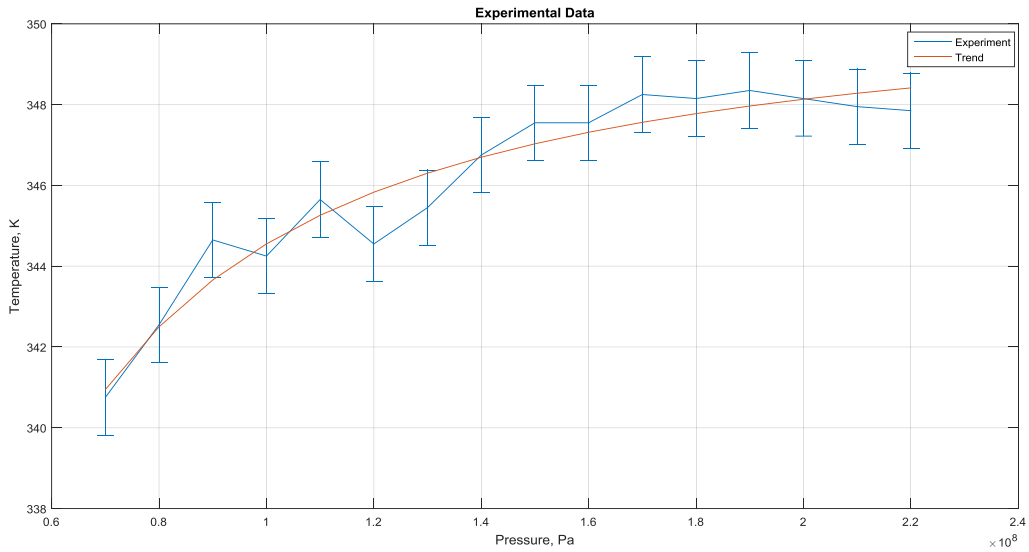


Figure 7.11.1.1.1

As seen in figure 7.11.1.1.1, a clear trend line appears on the temperature outlet plot, and this trend line is showed in the plot in orange color. The sudden bumps in temperature at the range of 9-12 MPa occur due to adjustments of the fluid flow, because of the inability of the pump to stabilize the pressure at specified pressure. This experiment showed that the taking readings from heat exchanger wall temperature is a valid approximation, as the trend of the outlet temperature stays the same, although there might be some deviations in readings in the lower pressure regions.

### 7.11.1.2 2<sup>nd</sup> Heat Exchanger

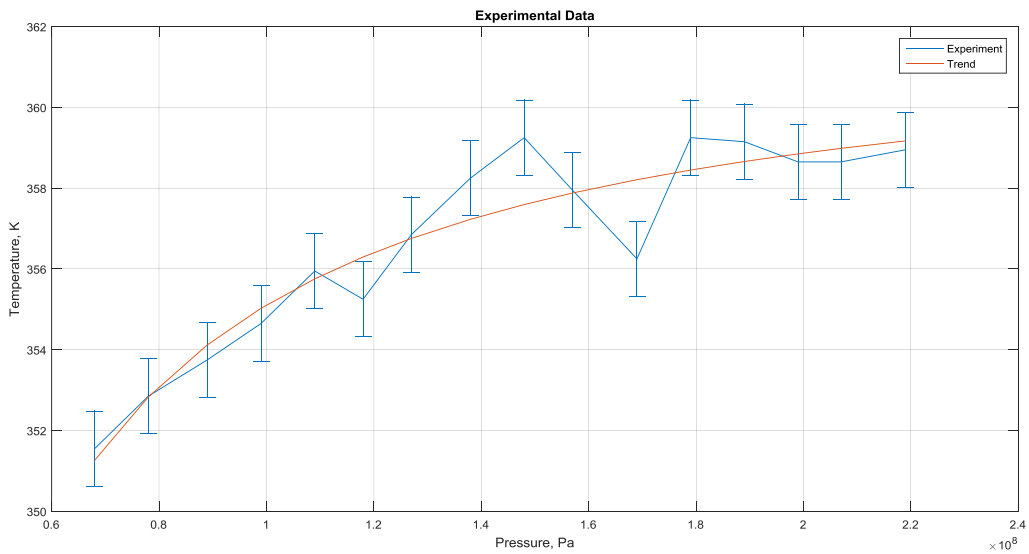


Figure 7.11.1.2.1

The same trend appears to be valid and for the 2<sup>nd</sup> heat exchanger (figure 7.11.1.2.1), and the sharp variations in temperature are attributed to adjustments to the flow of gas in order to stabilize the working pressure. In this data set, however it is possible to notice that there is no temperature decrease at the pressure is raised above 20 MPa, which gives rise to confidence that this set is the most precise one attained.

## 7.11.2 Analysis

### 7.11.2.1 1<sup>st</sup> Heat Exchanger

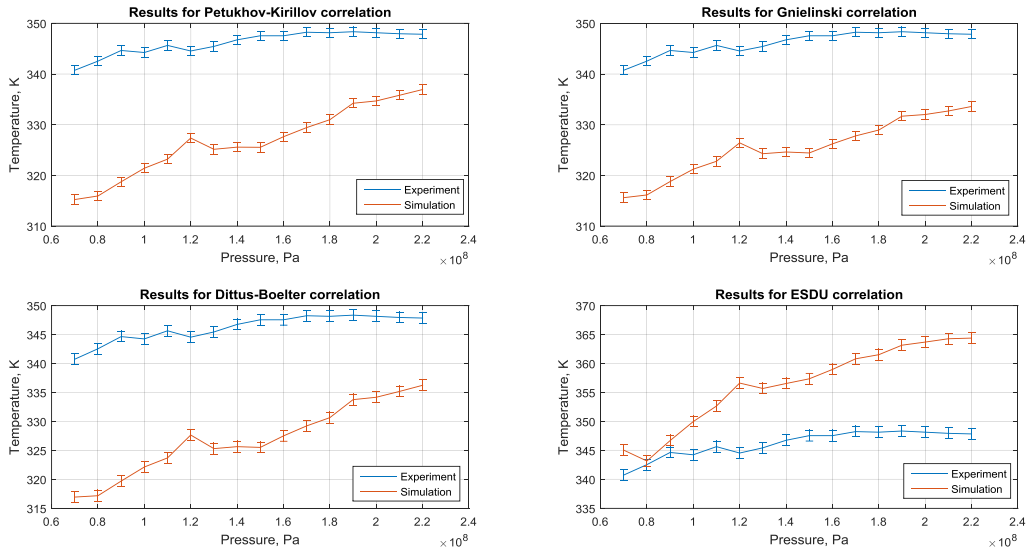


Figure 7.11.2.1.1

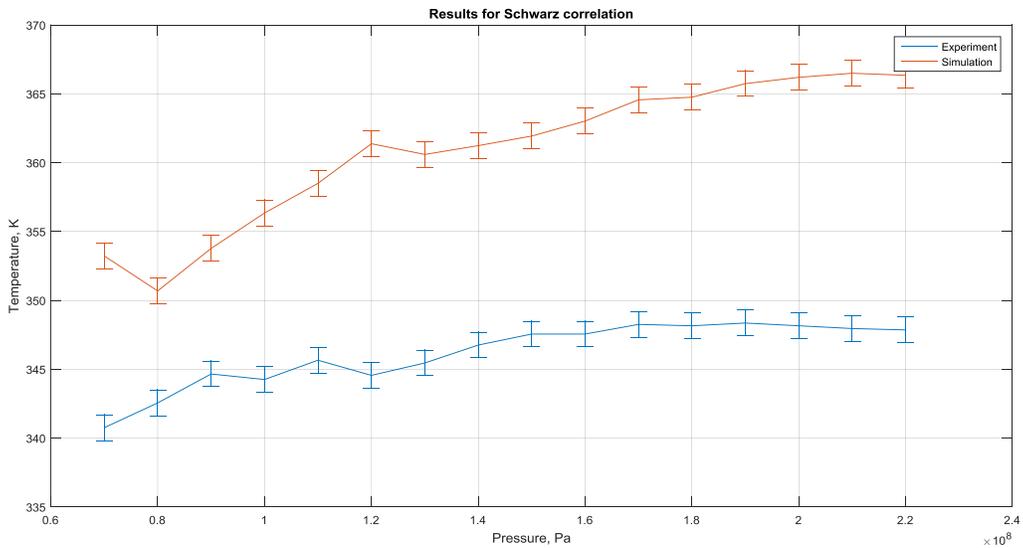


Figure 7.11.2.1.2

As seen from the figures (figure 7.11.2.1.1 and figure 7.11.2.1.2), all of the equations fail to predict the heat transfer in the heat exchanger when the fluid passes through the supercritical point, which can be seen on the RMSE table. Even though FluidProp software accurately predicts the heat capacity of the fluid when it passes through the supercritical point, still the discrepancies between experiment and simulation are quite big. Surprisingly, the correlations that produce results that correlate best with the experiment are the ESDU and Schwarz correlations, though it is speculated that it is only a coincidence that there is a match, and the results can be interpreted as being false positive. However, even though the algorithm fails to predict the heat transfer in the heat exchanger with phase change, it is not a big issue, due to the fact that the power generating station will be operating with a fully supercritical cycle, where no phase changes occur and the full cycle is supercritical.

HX 1		
Model	RMSE	
	7-16 MPa	7-22 MPa
PK	22.6	20.0
GL	23.0	21.0
DB	22.0	19.7
ESDU	8.2	11.2
SWZ	13.4	15.1

Table 7.11.2.1.1

Table 7.11.2.1.1 displays the RMSE of predictions of all the correlations used. As it is seen from this table, the Petukhov-Kirillo, Gnielinski and Dittus-Boelter correlations perform better when considering the full range of pressures tested, which means that the equations are more accurate when considering heat transfer at higher pressures. The explanation for this is that when the fluid goes through the critical temperature at high pressures, the sudden spikes in heat capacity are smaller the higher the pressure, which can be observed in figure 7.11.2.3.1.1. Having smaller/no peaks in heat capacity also means that fluid behavior is less unpredictable, and the simulations can be more reliable.

### 7.11.2.2 2<sup>nd</sup> Heat Exchanger

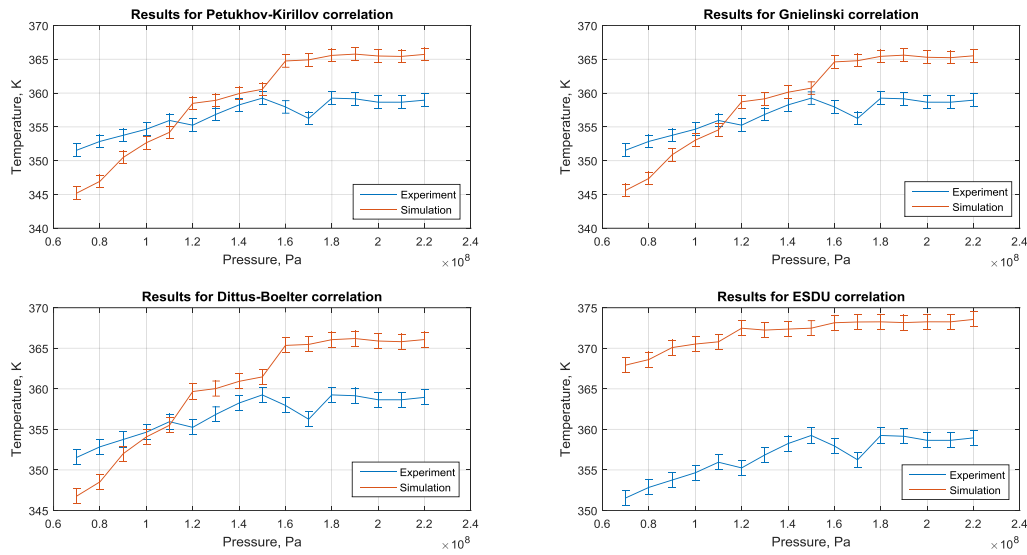


Figure 7.11.2.1.1

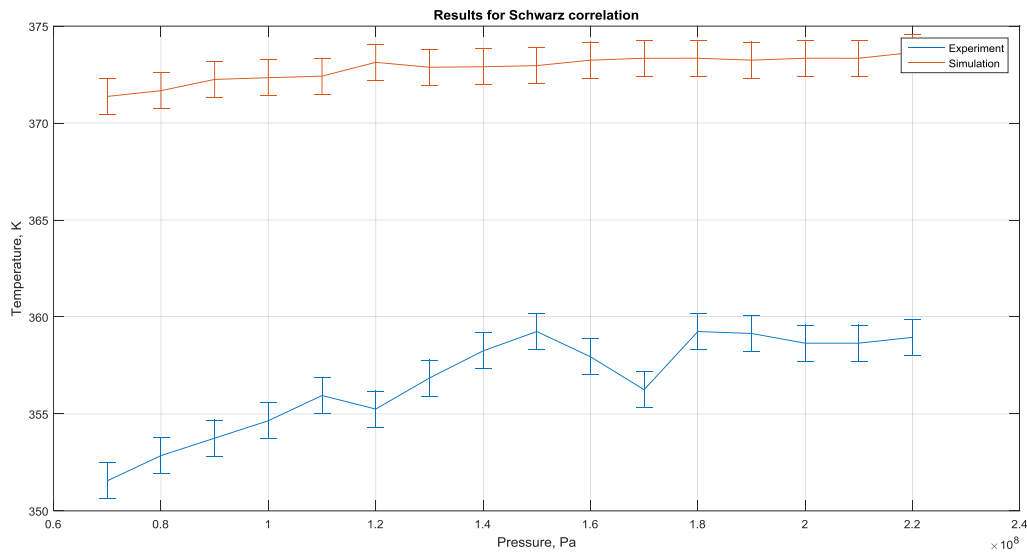


Figure 7.11.2.1.2

For the 2<sup>nd</sup> heat exchanger the picture (figure 7.11.2.1.1, figure 7.11.2.1.2) is totally different from what it is for the 1<sup>st</sup> heat exchanger, and this can be clearly seen from the RMSE table (table 7.11.2.1.1). When phase change is eliminated, the performance of the heat transfer correlations improves significantly. The Petukhov-Kirillov, Gnielinski and Dittus-Boelter correlations perform remarkably better for the fully supercritical heat exchanger than for the phase transitional one. Even though there are some discrepancies on the high and low pressure regions on the plot, for the full range of pressures for the said 3 heat transfer correlations the RMSE is around 5.3 °C, for the pressure range of interest (7-16 MPa) the RMSE is only about 3.8 °C, which is considered very accurate predictions of reality.

The ESDU and Schwarz correlations however have proven to be not useful for predicting the heat transfer coefficient, and their RMSE is around 3 times bigger than it is for the first 3 heat transfer correlations mentioned in this paragraph.

HX 2		
Model	RMSE	
	7-16 Mpa	7-22 Mpa
PK	4.0	5.3
GL	3.8	5.2
DB	3.8	5.5
ESDU	15.5	15.2
SWZ	17.0	16.2

Table 7.11.2.1.1

### 7.10.2.3 Fluid Behavior

#### 7.10.2.3.1 HX1

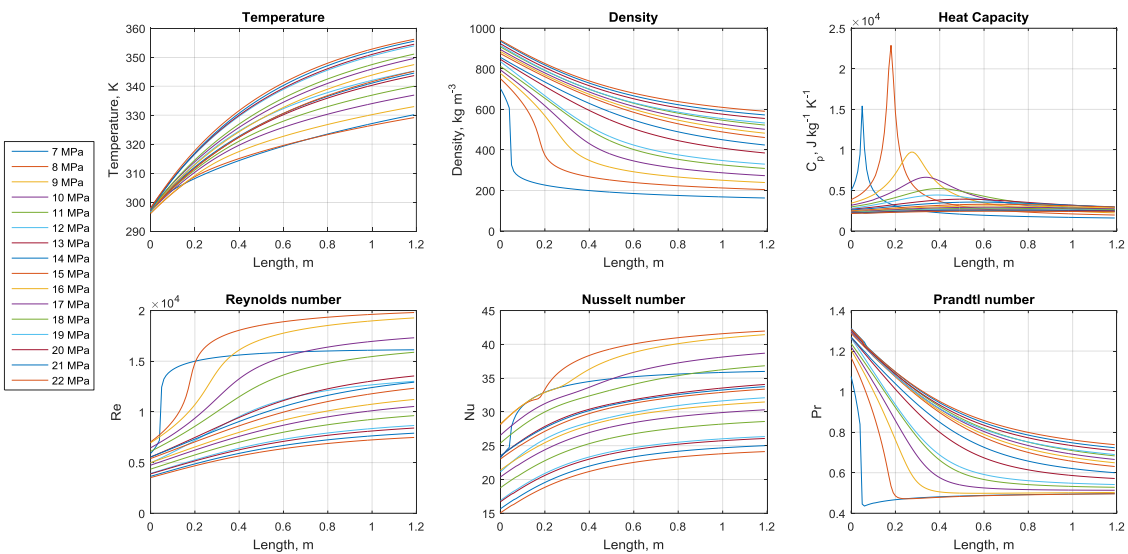


Figure 7.11.2.3.1.1

To graphically depict how fluid properties evolved, a plot showing key fluid features, as well as non dimensionless numbers has been created. To better match reality, the Gnielinski correlations was modified by a fudge factor to match experimental data up to an RMSE of 6.5 °C. The fudge factor added to the correlation is not suggested to improve performance of the equation in any case, as this was added just to better match experimental data for this particular case, to be able to demonstrate dynamics of fluid properties within the heat exchanger.

On the multiple plots that are displayed in the chart (figure 7.11.2.3.1.1), perhaps the most interesting one is the plot with heat capacities of the fluid, as here the state transition can be observed quite clearly, with large spikes indicating state transition. Even though the 7 MPa line is subcritical, the spike in heat capacity indicates liquid CO<sub>2</sub> is going through a state transition turning into vapor, with its heat capacity

falling as the fluid gets less dense, which can be seen on the density plot as well. All the other sharp peaks on the heat capacity plot indicate fluid state transition, and the largest spike can be observed for the fluid subjected to 8 MPa pressure. As the pressure is increased further, it can be observed that the state transition occurs at further down the heat exchanger, which indicates that at higher pressures the supercritical transition occurs at higher temperatures as well, and the change in fluid properties is also not that sharp (the supercritical fluid behavior displays more fluid like behavior, rather than gas like).

Analysis of the Reynolds number plot reveals that flows under almost all of the pressures tested are turbulent, with the minimum Reynolds number observed being around 4000. In this plot, the subcritical CO<sub>2</sub> line can be observed, with a sharp rise in the Re number, and staying almost constant throughout the heat exchanger. The other pressures exhibit behavior similar to the heat capacity one – with increasing pressure, the rise in Reynolds number happens more smoothly, and further down the heat exchanger.

The Nusselt number plot, as seen in the figure, has a minimum value of 15, which indicates that the convective heat transfer in the fluid is much more important than the conductive one, but it is noted that as the pressure is increased, the role of conduction in heat transfer for the fluid plays a greater role, as on the plot it is seen that as the pressure is increased, the Nusselt number tends to drop.

Finally, analysis of Prandtl number shows that as the fluid enters the heat exchanger, the dominating force inside of the fluid is the momentum diffusivity, as the value of Pr is >1, but as the fluid passes through the heat exchanger, the Pr tends toward a single value, which is somewhere around the region of 0.5-0.7.

#### 7.11.2.3.2 HX2

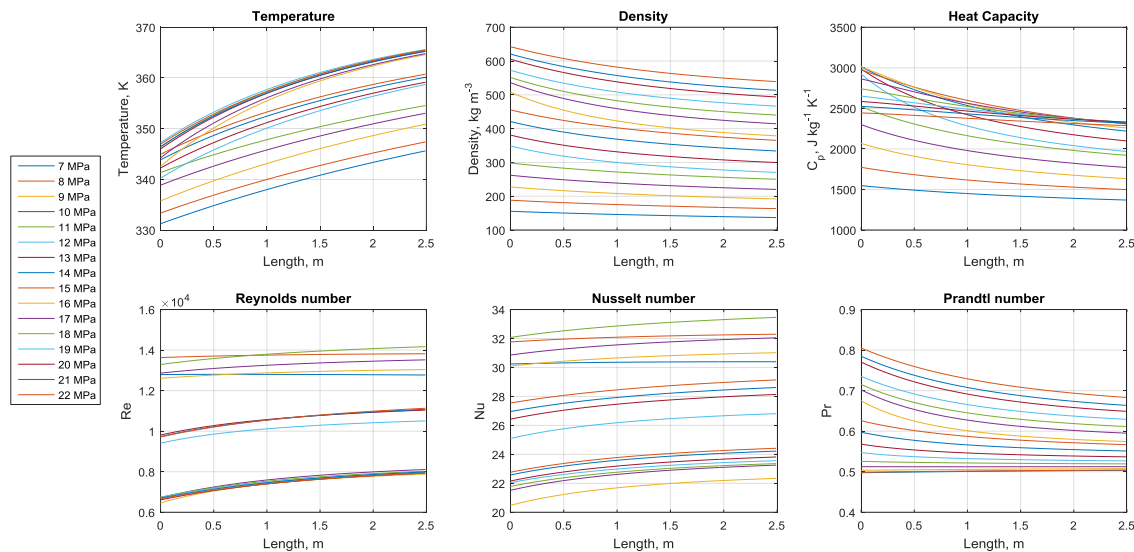


Figure 7.11.2.3.2.1

As seen on the fluid property dynamics plot of the supercritical heat exchanger, it can be seen that the properties of the fluids change in a lot more linear manner than the phase transitional heat exchanger, and this is one of the possible reasons as to why the predicted results are a lot closer to experimental results.

The heat capacity, as seen on the plot, increases up to about 12 MPa quite fast, rising from about 1500 to 3000 J kg<sup>-1</sup> K<sup>-1</sup>, after which the changes in the heat capacity tends to be less evident, i.e. becoming more linear.

The density also can be seen as displaying a more linear behavior, though at higher pressures the change in density as the fluid goes through the heat exchanger is greater than at lower pressures.

On the Reynolds number plot, 4 distinct groups of lines can be seen, and this is attributed to manually modifying the mass flow of the system in order to help the pump achieve stable pressure.

On the Nusselt number plot the trend tends to be the same as in the transitional heat exchanger – as pressure is increased, the thermal conduction starts to play a greater role, though as the fluid passes through the heat exchanger, convection starts to take a greater role.

Finally, the Prandtl number plot shows that thermal diffusivity is the dominating force over the momentum diffusivity, as all the tested pressures have a Prandtl number less than one. And although the Prandtl number is less than one, it is not too far away from one (with the smallest value being around 0.5), which suggests that momentum and thermal diffusivities are approximately equally important for the fluid.

## 7.12 Pressure Drop

While conducting experiments an unusual fluid behavior has been noticed – an unexpectedly large pressure drop – at some flows the pressure drop reached up to 7±1 bar. This unusual behavior continued for as long as the experiment was run with the initial configuration.

After reconfiguring the experiment with inserting thermocouples into the fluid stream and taking extra effort to make the entrance ducts into the heat exchanger smooth, the large pressure drop disappeared, and it became impossible to notice the pressure drop, as it was smaller than the error of readings on the pressure gauges (<1 bar). Therefore it has been concluded that the pressure drop was caused by obstruction by metal shavings inside or on the inlet of the heat exchanger. Therefore, if taking into account that the experiments were run with pressures reaching 22 MPa, and the pressure drop was below 0.1 MPa, it can be assumed that heat exchange happened at constant pressure.

## 7.13 Conclusion for the experimental section

After performing many experiments and obtaining a large amount of experimental data and testing different heat transfer correlations, a number of conclusions have been made.

From the 5 tested correlations, the Petukhov-Kirillov, Gnielinski, Dittus-Boelter, ESDU and Schwarz, it has been concluded that the first three correlation outperform the last two, and all three correlations can be used with similar errors of prediction.

Although all three correlations have performed similarly, the Gnielinski correlation has been found to give the most precise results, following by the Petukhov-Kirillov correlation, closely followed by the one proposed by Dittus-Boelter. Therefore a decision has been made to incorporate the Gnielinski correlation in the simulation of the geothermal heat exchanger. However, if computational power is a problem, the Dittus-Boelter correlation should be used, due to its simplicity compared to the Gnielinski correlation.

It has also been concluded that these correlations have a limit of applicability with the temperature differences that are operated at. The experiments have showed, that if a heating medium that has a higher than water temperature (PEG for example), the correlations tend to fail in predicting the heat exchanger performance and generate results that are far away from reality. Also, even though the correlations perform well in predicting fluid heating heat transfer, the performance is poor when considering cooling the liquid with ice water, as there the equations underestimate the heat transfer coefficient, and predicting results with a much higher fluid outlet temperature than experiments suggest.

Another conclusion that has been attained, is that the algorithm performs poorly when it comes to predicting fluid properties when the supercritical point is passed. Simulations have showed around 20 °C RMSE when the heat exchanger with state transition is simulated, compared to about 5 °C when no state transition is occurring, therefore caution should be taken when considering modelling a heat exchanger with a transition through the supercritical region.

## 8 Geothermal Plant Simulation

### 8.1 Simulation Requirements

To simulate this power production system, a number of effects need to be taken into consideration. 1<sup>st</sup> of all, because the supercritical fluid moves vertically down through the column, it gets compressed (because supercritical fluids are easily compressible). The compression of the fluid in turn raises the fluid temperature, which results in a decreased density, and this compression/expansion effect needs to be carefully controlled. The motion of the fluid down through the column is governed by fluid mechanics (pressure drop caused by the motion of the fluid, as well as buoyancy forces due to a pressure, temperature and density gradient). Down at the heat exchanger, other thermodynamic effect take place – conduction and convection, which govern fluid heat exchange. This effect in turn causes a change in the fluid properties, which needs to be taken into account in order to accurately model the system.

The resulting simulation therefore represents a system of equations which take into account thermodynamic and fluid mechanic effects.

### 8.2 Assumptions

To build the system, a number of assumptions need to be made:

- Depth of the heat exchange in the system is 1000 m below ground level
- CO<sub>2</sub> loop is closed
- CO<sub>2</sub> remains supercritical throughout the cycle
- The main driving force is density difference (buoyancy)
- Mass flow is constant throughout the system
- On small enough distances fluid properties behave in a linear manner
- Energy is extracted from the system using a positive displacement pump

Using these assumptions, it is possible to build a model of the system.

After carrying out the experiments in determining the best possible heat transfer correlations, as well as determining the error of predictions in the simulation, the creation of a full scale simulation has been completed using the attained data. For the simulation a step size of 1 meter has been selected, since on these scales fluid property dynamics are approximately linear when considering the full length of the pipe

used in the simulation (1000 m). The developed algorithm considers 5 key places in a power generating cycle – transportation pipes (down and up), as well as bottom and surface heat exchangers, and the most importantly – the positive displacement pump (PDP), a unit which generates power in this system.

Although most of the equations used in the simulation give reliable results with little deviations from experiment, the PDP equations are fully theoretical, and give a theoretical result based on 100% efficient pump. Unfortunately, it is not possible to provide more accurate results, since the pump efficiency depends on a lot of factors that can't be generalized upon (vane tolerance, size, pump type, etc.)

The algorithm developed gives predictions of fluid properties such as fluid density, pressure, velocity, viscosity, buoyancy forces, as well as a number of non-dimensional numbers (Prandtl, Grashof, Reynolds and Nusselt).

As the simulation also takes into account the physical aspects of the system, such as the heat exchanger design, this turned out to be a key factor in determining the heat transfer coefficient. Simulations have showed that the best results are achieved when the heat exchanger is modelled as a U-tube heat exchanger, with multiple small diameter pipes. The best achieved results were with an internal pipe diameter of 2 cm, and an outer diameter of 3.175 cm, and 30 pipes. In this case the required length of pipe used was estimated to be 10 m, and assuming that the heat exchanger is a U-tube design, the actual length of the heat exchanger would be 5 m.

The system design was based on a constant mass flow of CO<sub>2</sub> across the entire plant. This was taken into account when determining the length of the heat exchanger. It has been noted, that there is a tradeoff between the mass flow in the system and the power that the system that is able to generate. Higher mass flows in the pipes imply higher fluid velocity, and this in turn causes a larger pressure drop. As well as the pressure drop in the transportation pipes, pressure drop considerations need to be made when designing the heat exchanger. Since the heat exchanger utilizes quite small pipes for heat exchange in comparison with the transportation pipes, the pressure drop experienced by the fluid is going to be significant if an excessive length of the heat exchanger is used, therefore under selected parameters, the best performance is achieved when a 10 m length of heat exchanger is used, with a mass flow of 12 kg s<sup>-1</sup>.

### 8.3 System Specifications

The system was designed with the following specifications:

Parameter	Value	Units
Well Diameter	0.3	m
Well Length	1000	m
Well Water T	90	°C
Well Water Flow	200	m <sup>3</sup> hr <sup>-1</sup>
Cold Pipe ID	0.12	m
Hot Pipe ID	0.12	m
HX Pipe ID	0.02	m
N of HX Pipes	25	
Max T of CO <sub>2</sub>	350 (77)	K (°C)
Min T of CO <sub>2</sub>	305 (32)	K (°C)
Mass Flow of CO <sub>2</sub>	12	kg s <sup>-1</sup>

Choke Pressure	8	MPa
----------------	---	-----

### 8.4 System Performance

The 1<sup>st</sup> part of this chapter will be discussing fluid dynamics in the transportation pipes, after which the attention will be given to the heat exchangers, and finally the final result of the theoretical power output will be presented.

#### 8.4.1 Transportation Pipes

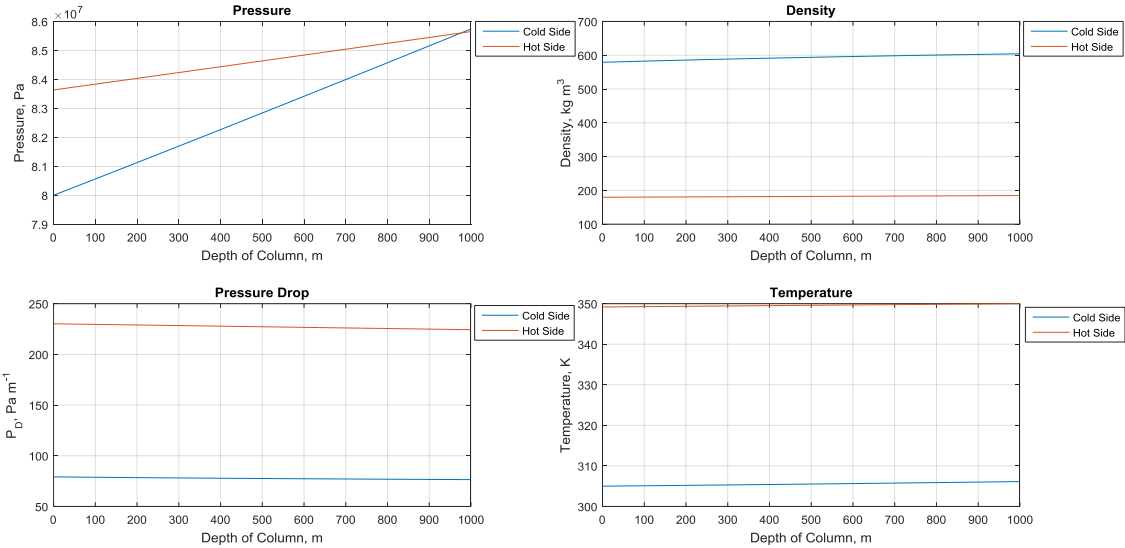


Figure 8.4.1.1

Multiple simulations have been performed in order to determine the best mass flow and operating pressure vs the power output generated by the system. It is favorable for system to operate at the lowest possible pressure, yet at the same time the highest possible mass flow. Lower operating pressures are favored for this system in order to minimize the thickness of the pipes used for transportation of CO<sub>2</sub> from the surface to the bottom heat exchanger. This is why an operating pressure of 8 MPa has been chosen as the choke pressure at the top of the cold column. Choosing this pressure would provide a margin safety of around 0.5 MPa above the critical pressure of CO<sub>2</sub>, both at the same time allowing a high mass flowrate of around 12 kg s<sup>-1</sup>. As seen in figure 8.4.1.1, having CO<sub>2</sub> at an inlet pressure of 8 MPa and a temperature of 305 K, the density of the fluid remains at about 600 kg m<sup>-3</sup>. With the depth of the column being 1000 m, the hydrostatic pressure of the column of the fluid turns out to be around 0.4 MPa, or 4 bar. The density plot shows that the fluid density during its descend down the column changes increases only slightly, though the hydrostatic pressure increase is quite significant. The reason as to why there's such little density increase in the fluid is explained by adiabatic fluid expansion, and hydrostatic fluid compression. Since a 1 cm layer of insulation is used for the transportation pipes in order to minimize fluid heat exchange with the surrounding water, the pipe can be considered as near-ideal adiabatic, i.e. it does no experience heat exchange with its surroundings. Due to this when the fluid is compressed it generates heat, expands, and balances the compressive forces. Also, although the pipe is considered to be adiabatic, it's not fully true, as the insulation is not perfect ( $\lambda=0.02 \text{ W m}^{-1} \text{ K}^{-1}$ ), and therefore the fluid experiences around 2 °C increase in temperature due to heat exchange with its surroundings. As seen on the pressure drop plot, the hot CO<sub>2</sub> experiences almost 4 times the pressure drop that the cold side does. This is due

to the density difference on both sides, and correspondingly the velocity on both sides. Pressure drop in this project is considered as a limiting factor for power generation.

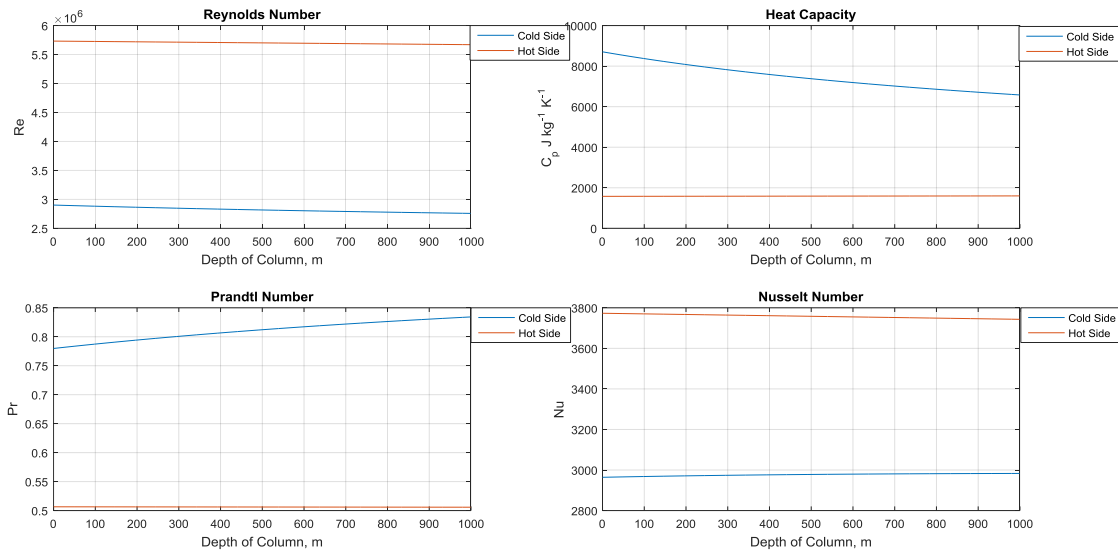


Figure 8.4.1.2

As seen in figure 8.4.1.2, the Reynolds number is much higher for the hot fluid pipe than it is for the cold fluid one. This is due to the hot fluid side being a lot less dense and since the mass flow in both pipes are the same, a much higher velocity (around 3.5 times higher). A consideration was taken on making the cold pipe diameter smaller than the hot pipe, but simulations have showed that this would cause a greater pressure drop, and therefore a smaller pressure at the bottom heat exchanger, and thus would result in smaller power output out of the system.

On the heat capacity plot it is seen that the cold side pipe has a much higher heat capacity than the hot side, and this is due to the fluid on the cold side being much closer to the critical point than the hot side. Also, due to this fact the change in the heat capacity is much larger than it is for the hot fluid. The fact that the cold fluid has such a high heat capacity also means that the bottom heat exchanger is going to substantially lower the well water temperature when it passes through it.

On the Prandtl number plot it is seen that the cold side has a higher Prandtl number value than the hot side does. However, both of these values are less than 1, and a Prandtl value of less than 1 indicates that thermal diffusivity is the dominating force over momentum diffusivity.

On the Nusselt number plot it is seen that the picture is a complete opposite of the Prandtl number plot. Since the Nusselt number is an approximation of the ratio of convective to conductive heat transfer, it is seen that the convection heat transfer is higher on the hot side, and conduction is more important for the cold pipe fluid, although the values are quite close. This can be attributed to a higher density of the fluid in the cold well. Due to this effect, the length of the bottom heat exchanger required to achieve the required temperature rise will be smaller than for the surface heat exchanger.

## 8.4.2 Heat Exchangers

### 8.4.2.1 Bottom Heat Exchanger

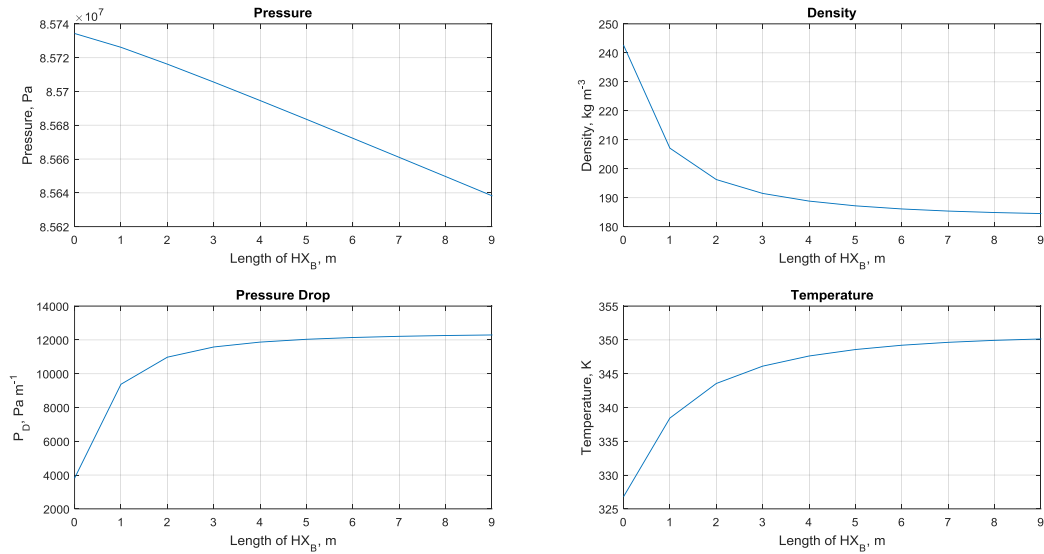


Figure 8.4.2.1.1

The 1<sup>st</sup> heat exchanger described in this chapter is the bottom heat exchanger. Calculations have showed that the length of the heat exchanger required to achieve the maximum possible temperature is 9 m, which means that if taken into account that the design of the heat exchanger is a U-tube heat exchanger, would make a practical length of around 5, if different fittings are to be installed on the heat exchanger. As seen on the density, pressure drop and temperature plot (figure 8.4.2.1.1), significant changes to the properties of the fluid occur up to about 4-5 m length of the heat exchanger, after which only minor changes occur. This is because of the mass flow of the supercritical fluid compared to the mass flow of water that passes through the heat exchanger. Figure 8.4.2.1.2 presents a plot of the water temperature as it passes through the heat exchanger.

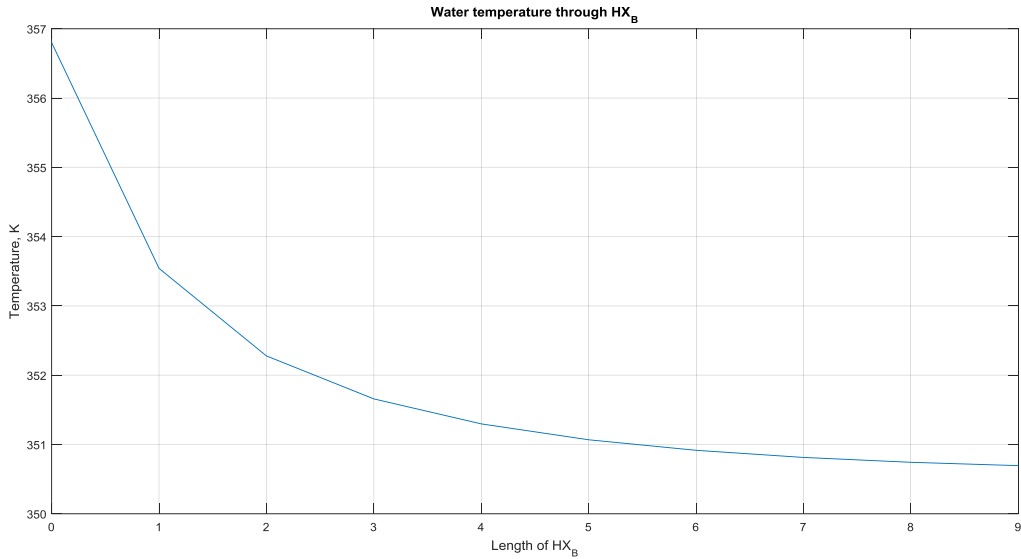


Figure 8.4.2.1.2

As seen in figure 8.4.2.1.2, the heat exchanger causes quite a big change in the water temperature, and this is attributed to a quite high heat capacity of the supercritical fluid, which will be discussed later. Assuming that the geothermal source allows the water to heat up to 363 K (90 °C), the temperature drop experienced by the water is around 13 °C, which means that if the system is to be retrofitted into an existing hydrothermal well that is used for district heating, it's heating ability will be lowered.

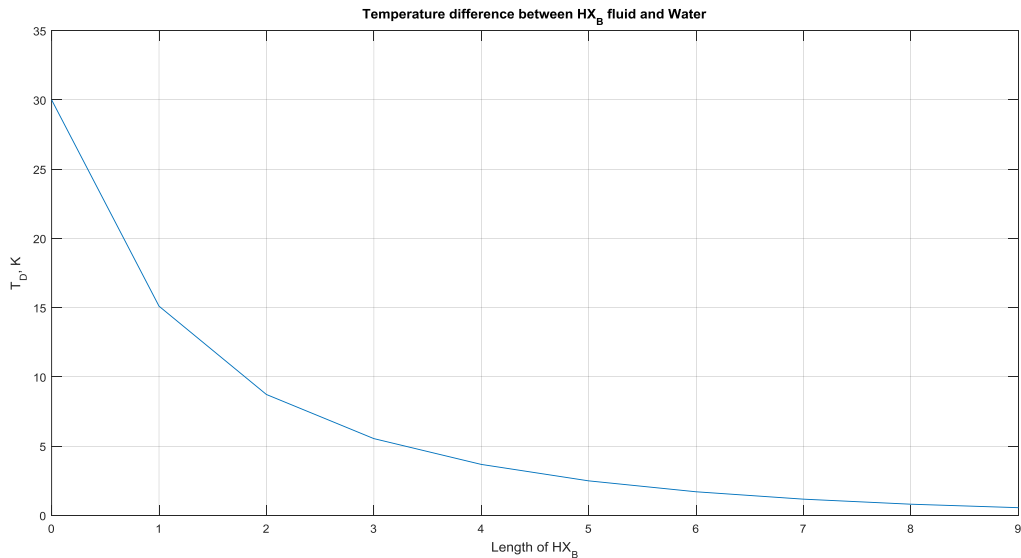


Figure 8.4.2.1.3

On this plot (figure 8.4.2.1.3) the temperature difference between the water and the heat exchanger fluid is plotted. As it is seen from the plot, the temperature difference drops exponentially, and therefore all the rate of heat transfer will also change exponentially, resulting in much smaller heat transfer rates toward the end of the heat exchanger. Coulson & Richardson (39) states that for design purposes when performing pressure drop calculations the equation needs to be multiplied by a factor of 8 to have realistic

pressure drop values. As seen on the pressure drop plot, the pressure drop experienced by the fluid inside of the heat exchanger reaches a maximum value of 0.12 bar, and this is the reason as to why the length of the heat exchanger needs to be minimized when performing sizing calculations.

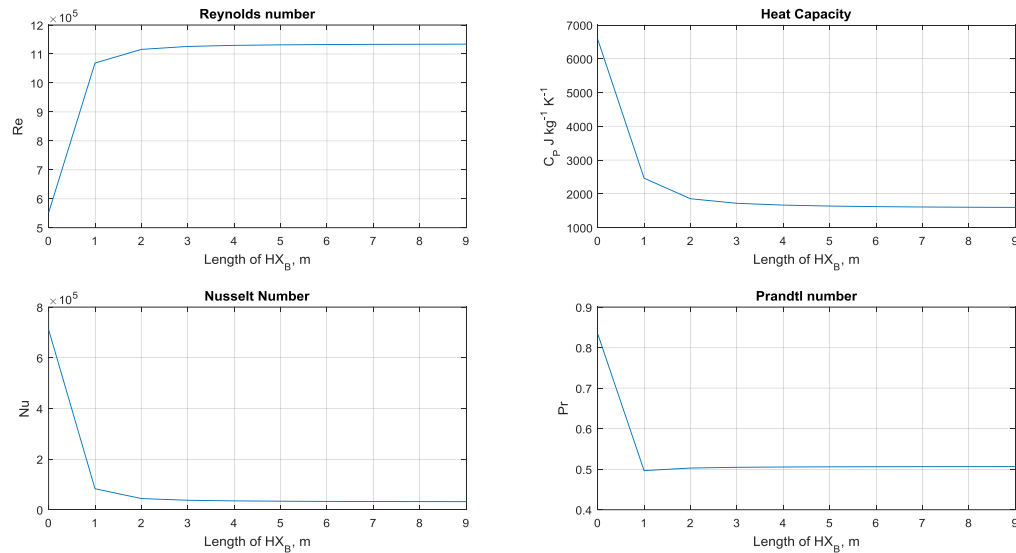


Figure 8.4.2.1.4

As for the fluid properties, figure 8.4.2.1.4, on all of the plots it's possible to see that most of the changes experienced by the fluid are happening in the first 2-3 meters of the heat exchanger, after which they reach a nearly stable value. On the temperature difference plot it can be seen that that corresponds to a temperature difference between the fluid and the water of about 10 °C.

#### 8.4.2.2 Surface Heat Exchanger

As it has been determined from the experimental section, the design of a cooling heat exchanger is subjected to critique, to when considering the experimental evidence that the Gnielinski correlation does not perform well when considering supercritical fluid cooling. However, theoretical results suggest that the required length of the heat exchanger is to be 11 m, if taken into account that the heat exchanger is to be of a U-tube design. Although the simulation shows that the required length of the heat exchanger for this case is 11 m, experiments have shown that there might be an underestimation of the heat transfer coefficient, and therefore the real length of the heat exchanger can be even shorter. Since this heat exchanger is located at the surface of the plant, space is not a limiting factor, therefore multiple design solutions can be implemented. For this project however, a U-tube design will be considered. The cooling fluid for this project was selected to be water with a temperature of 8 °C, and since various water sources are available with various mass flowrates, no temperature change of water will be considered, as this topic is very subjective to individual well designs.

The basic outline of the heat exchanger for this project is going to be identical to the bottom heat exchanger – 2 cm ID pipes having a 3.175 cm OD, and 30 pipes bent into a U shape.

It has been determined from simulations that the efficiency of the plant depends on the length of the bottom heat exchanger. However not only the bottom heat exchanger length should be minimized, as the same can be said for the surface heat exchanger. A shorted heat exchanger would mean less pressure

drop occurring though it, and therefore the positive displacement pump outlet pressure can be lower, and therefore more energy can be extracted from the fluid.

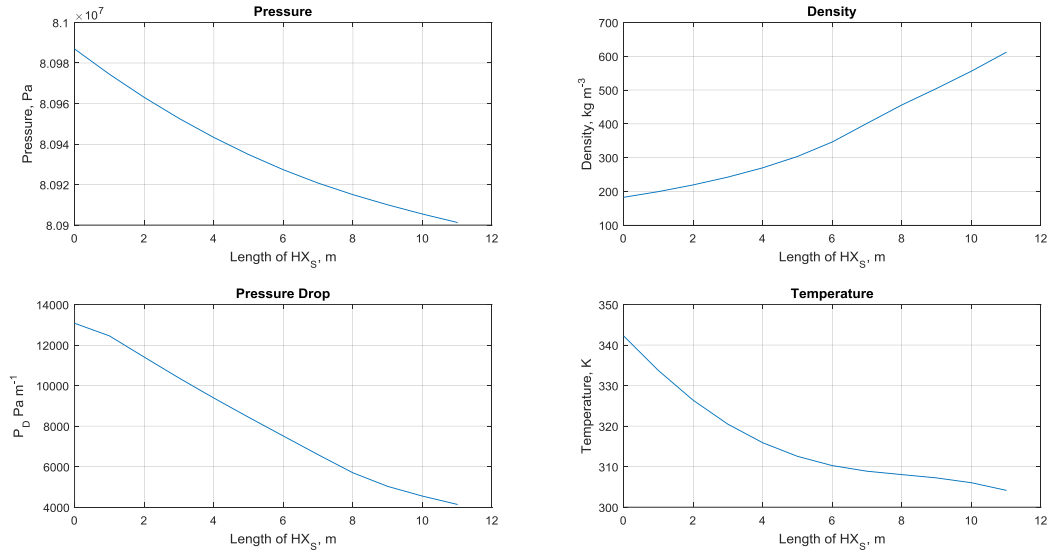


Figure 8.4.2.2.1

As simulations have shown, and what can be seen in the figure 8.4.2.2.1, the length of the heat exchanger required to cool the fluid down to 305 K (32 °C) is 11 m. Also it is possible to see that the fluid properties in the heat exchanger are changing not so rapidly as they do for the bottom heat exchanger. This is partially because of the simulation assumption that the water temperature stays constant. It is also possible to observe that apart from the pressure inside of the heat exchanger, all the other system parameters (fluid temperature, density and pressure drop) do not follow the classic exponential style dynamics in fluid properties as observed in all the other figures and graphs. And this is attributed to the supercritical fluid heat capacity, which can be observed in the figure below.

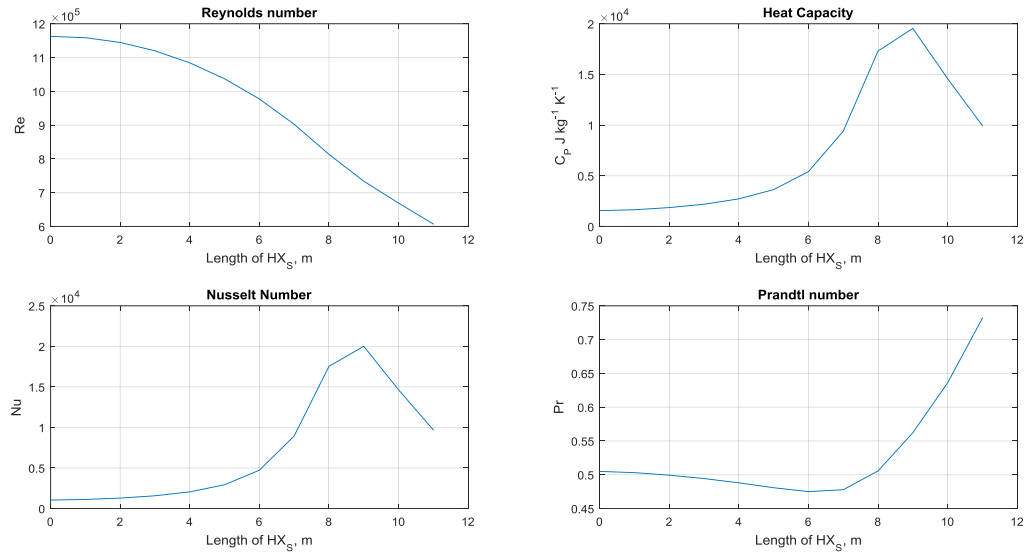


Figure 8.4.2.2.2

As seen of the fluid property (and non-dimensional number) plot (figure 8.4.2.2.2), as the fluid is cooled down to a point which is very close to the critical point, a sharp spike in heat capacity is observed towards the end of the heat exchanger, which in turn produces an increase in the change of fluid properties. This low temperature for the fluid was selected to maximize the power production of the plant, as the bigger the temperature difference is between the hot and cold side of the system, the more power it is capable to generate.

### 8.4.3 Grashof Number and Buoyancy Forces

When evaluating the system performance, attention was given to the buoyancy force that the fluid experiences inside the system, and the buoyancy force is evaluated by the non-dimensional Grashof number correlation with Reynolds number.

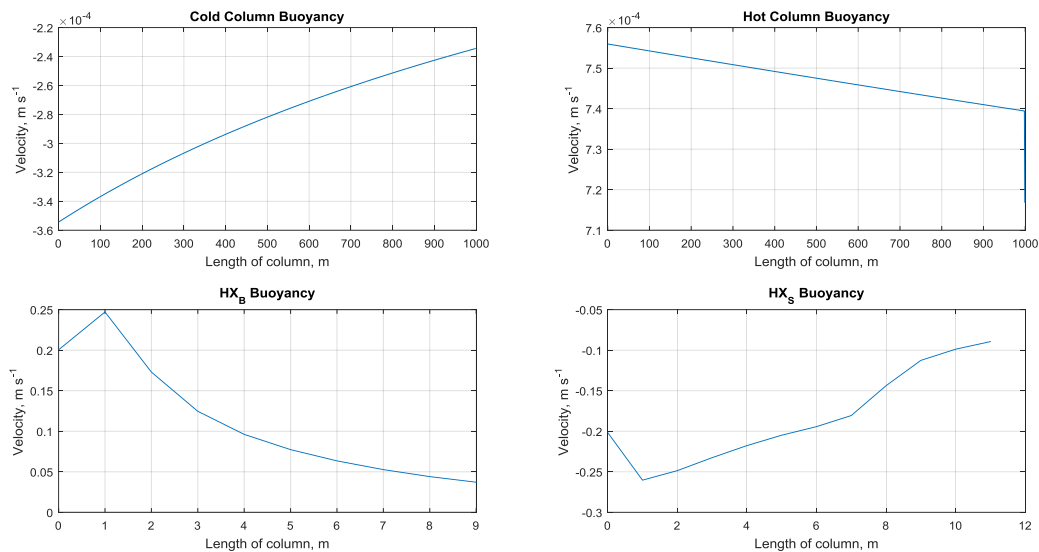


Figure 8.4.3.1

As seen in figure 8.4.3.1, the buoyancy forces are practically negligible, as the buoyancy induced velocity in the fluid in the transportation pipes are in the range of  $1 \text{ cm s}^{-1}$  or less, therefore the buoyancy force can be neglected in the transportation pipes. The negative values on the plot indicate that the buoyancy forces are acting against the flow, and positive that they acting the same way the flow does. The explanation for such small buoyancy forces in the transportation pipes can be spotted in Figure 8.4.1.1, the density plot. If looked at that plot, it is seen that the density change in the fluid going down the column is very small. And since in this case the fluid is pure, so there is no concentration gradient to drive the buoyancy force, the only possible driving force is the density difference, which as seen in figure 8.4.1.1 is very small, thus resulting in very small buoyancy induced velocity.

The buoyancy force in the cold and hot columns are very straightforward in understanding, with the buoyancy force counteracting the cold fluid descend down the column, and aiding the hot fluid to rise up the pipe, and as seen on the plot, the buoyancy force is more significant for the hot side, due to the fluid having less density. A more interesting picture arises in the buoyancy force in the heat exchangers. In the bottom heat exchanger the buoyancy force appears to be a significant contributing factor, increasing the velocity up to  $0.25 \text{ m s}^{-1}$ , though the contribution seems to drop as it continues to pass through the heat exchanger. This is because of the rapid drop in the temperature difference between the fluid and its surroundings, which implies less density change and therefore less buoyancy driven flow. A similar but opposite picture is obtained in the surface heat exchanger, when the entering fluid is velocity is retarded by the buoyancy force. And again a similarity arises with the bottom heat exchanger, when the temperature difference driving force drops, the buoyancy force ceases to play a significant role in the fluid flow. A conclusion has been made that although the buoyancy force has its place in the system and its effect is noticeable in the heat exchangers, the overall picture of the buoyancy effects on the system shows that it has an insignificant effect, and therefore can be neglected.

## 8.5 Power output

Simulations have shown, that under given design specification, the system can generate somewhere between 156 and 167.2 kW of energy, assuming 100% pump efficiency and an uncertainty of the fluid temperature of about 3 °C. A more precise figure however can't be given due to the fact that pump efficiencies depend upon a lot of factors which can't be included in this simulation, due to individual specifications of different pumps.

The power generation for this system can be greatly increased if the diameter of the well drilled can be increased, which would then allow fitting of a bigger heat exchanger and larger diameter transportation pipes. For example, having the same system configuration, but changing the transportation pipe ID to 0.15 m, and increasing the flow of CO<sub>2</sub> to 16 kg s<sup>-1</sup>, and the number of pipes in the bottom heat exchanger to 40, would produce a power yield between 200 and 235 kW. The drawback however is that the water pumping rate through the heat exchanger needs to be increased in order to produce the same temperature rise in the fluid as was done with the 30 cm well diameter system. This can have additional pumping costs, as the increased water flow will require more pumping power.

## 8.6 Commissioning

Calculation showed that natural velocity in this system is too small to play a significant role in fluid flow in this system, which means that without an initial pulse the system will remain static, with no fluid circulation or power generation. Therefore commissioning of the plant will require initial energy input into the system to induce fluid circulation. This can be done by using the same equipment that is used for power generation.

After the start of forced fluid circulation, the pump then can be switched from pumping mode to power generation mode. After switching the motor power generation mode, the main driving force will be the density difference on the both sides of the pump (and a pressure difference because of that).

This can be explained by Bernoulli's equation. In its simplest form it can be written down as

$$P_1 + \frac{1}{2}\rho_1 V_1^2 + \rho_1 g h_1 = P_2 + \frac{1}{2}\rho_2 V_2^2 + \rho_2 g h_2$$

Because the pump is located horizontally, therefore the contribution of hydrostatic pressure will be negligible, therefore the whole term of hydrostatic pressure will be omitted.

$$P_1 + \frac{1}{2}\rho_1 V_1^2 = P_2 + \frac{1}{2}\rho_2 V_2^2$$

And rearranging equation in an explicit form to give V<sub>2</sub> therefore will give us

$$V_2 = \sqrt{\frac{2(P_1 - P_2) + \rho_1 V_1^2}{\rho_2}}$$

Where V<sub>2</sub> is the velocity of the fluid exiting the pump. The rest of the fluid will be driven by this pulse, the hydrostatic force, and a small contribution from the buoyancy induced convection.

## 8.7 Conclusion

The use of supercritical CO<sub>2</sub> for generating power from sub-boiling water hydrothermal wells in total has been evaluated as a viable method of energy production, with a typical sub-boiling well capable of producing a power output up to 167 kW, based on a 100% efficiency (which is around 600 MW h<sup>-1</sup>).

The limiting factor for efficient use of this system has been determined to be the transportation pipe internal diameter, and the pipe roughness. Extensive simulation have shown that if small diameter pipes and large fluid mass flows are used to generate power, the pressure drop generated by the moving fluid overpowers the hydrostatic force of the fluid, which causes a drop in pressure instead of an increase, which leads to decreased performance. Therefore, selection of pipe material, as well as diameter is crucial for successful implementation of the system.

Also, a drawback for this system is that if the well is also used for district heating or other kind of heating applications, the heating capacity will be decreased due to produced hydrothermal water temperature drop. However, if a larger well is drilled specifically for the implementation of this cycle, and a larger well diameter is selected, the system can generate more power than the ones that can be retrofitted into existing hydrothermal wells. The down side of the system however is that the cost of startup will be significant, as to the amount of CO<sub>2</sub> required to build up the required pressure in the system will be very big, and the startup of the system requires energy input. This problem however, can be solved by a variation of a CCS (carbon capture and storage). Since this technology uses pure CO<sub>2</sub>, which is produced by power generating systems, it is possible to obtain large quantities of CO<sub>2</sub> from the power industry, and utilize it in this project.

As simulations, as well as experimental data showed, supercritical CO<sub>2</sub> heat exchangers are an effective way to produce energy from hydrothermal wells.

## References

1. Lay, Thorne, Hernlund, John and Buffett, Bruce A. (2008), "Core–mantle boundary heat flow", *Nature Geoscience* 1: 25.
2. Geothermal capacity | About BP | BP Global, Bp.com, retrieved 2014-11-15.
3. Pahl, Greg (2007), *The Citizen-Powered Energy Handbook: Community Solutions to a Global Crisis*, Vermont: Chelsea Green Publishing.
4. Lund, John W., Freeston, Derek H. and Boyd, Tonya L. (24–29 April 2005), *World-Wide Direct Uses of Geothermal Energy 2005 (PDF)*, Proceedings World Geothermal Congress, Antalya, Turkey.
5. National Oceanic & Atmospheric Administration (NOAA) – Earth System Research Laboratory (ESRL), Trends in Carbon Dioxide Values given are dry air mole fractions expressed in parts per million (ppm). For an ideal gas mixture this is equivalent to parts pe.
6. Emden, Lorenzo. "Decaffeination 101: Four Ways to Decaffeinate Coffee". *Coffee Confidential*. Retrieved 29 October 2014.
7. Berche, Bertrand, Henkel, Malte and Kenna, Ralph (2009). "Critical phenomena: 150 years since Cagniard de la Tour". *Journal of Physical Studies* 13 (3): 3001–1–3001–4.
8. *Supercritical Fluid Extraction, Density Considerations*". Retrieved 2007-11-20.
9. *Hydrocarbons., U.S.EPA Method 3560 Supercritical Fluid Extraction of Total Recoverable*.
10. *applications", "Supercritical steam cycles for power generation*.
11. Agency, "Carbon Dioxide as a Fire Suppressant: Examining the Risks". U.S. Environmental Protection.
12. 2011-03-22., *International vocabulary of metrology — Basic and general concepts and associated terms (VIM)*. ISO. 2008. Retrieved.
13. Ting-Horng Chung, + Mohammad Ajlan,t Lloyd L. Lee,\* and Kenneth E. Starling. *Generalized Multiparameter Correlation for Nonpolar and Polar Fluid*.
14. Reynolds, Osborne (1883). "An experimental investigation of the circumstances which determine whether the motion of water shall be direct or sinuous, and of the law of resistance in parallel channels". *Philosophical Transactions of the Royal Society* 174 (.
15. Colebrook, C. F. (February 1939). "Turbulent flow in pipes, with particular reference to the transition region between smooth and rough pipe laws". *Journal of the Institution of Civil Engineers (London)*.
16. Colebrook, C. F. and White, C. M. (1937). "Experiments with Fluid Friction in Roughened Pipes".

17. Goudar, C.T., Sonnad, J.R. (August 2008). "Comparison of the iterative approximations of the Colebrook–White equation". Hydrocarbon Processing Fluid Flow and Rotating Equipment Special Report(August 2008): 79–83.
18. P.K. Swami, A.K. Jain, Explicit equations for pipeflow problems, J Hydraulics Div, Proc ASCE (1976), pp. 657–664 May.
19. <http://web2.clarkson.edu/projects/subramanian/ch302/notes/Convective%20Heat%20Transfer%201.pdf>.
20. Brkić, Dejan (2011). "An Explicit Approximation of Colebrook's equation for fluid flow friction factor". Petroleum Science and Technology 29 (15): 1596–1602.
21. Serghides, T.K (1984). "Estimate friction factor accurately". Chemical Engineering Journal 91(5): 63–64.
22. Brown, Glenn. "The Darcy-Weisbach Equation". Oklahoma State University–Stillwater.
23. [http://neo-classical-physics.info/uploads/3/0/6/5/3065888/caratheodory\\_-\\_thermodynamics.pdf](http://neo-classical-physics.info/uploads/3/0/6/5/3065888/caratheodory_-_thermodynamics.pdf).
24. Thomson, W. (1854). "On the Dynamical Theory of Heat. Part V. Thermo-electric Currents". Transactions of the Royal Society of Edinburgh 21 (part I): 123.
25. Perrot, Pierre (1998). A to Z of Thermodynamics. Oxford University Press. ISBN 0-19-856552-6.
26. Peng, D. Y., and Robinson, D. B. (1976). "A New Two-Constant Equation of State". Industrial and Engineering Chemistry: Fundamentals 15: 59–64.
27. Clausius, R. (1850), page 384, equation (IIa.).
28. S. Blundell, K. Blundell (2006). Concepts in Modern Physics. Oxford University Press. p. 247.
29. Suthan S. Suthersan, "Remediation engineering: design concepts", CRC Press, 1996.
30. Coulson, J. M. and Richardson, J. F. (1999). Chemical Engineering Volume 1 (6th ed.). Elsevier. ISBN 978-0-7506-4444-0.
31. Incropera, Frank P. and DeWitt, David P. (1990). Fundamentals of Heat and Mass Transfer (3rd ed.). John Wiley & Sons. p. 28. ISBN 0-471-51729-1. See Table 1.5.
32. <http://web2.clarkson.edu/projects/subramanian/ch302/notes/Natural%20Convection.pdf>.
33. 2015, "Convective Heat Transfer Convection Equation and Calculator". Engineers Edge. Retrieved 14 September.
34. Sanvicente, E. and 87–104., et al. (2012). "Transitional natural convection flow and heat transfer in an open channel". International Journal of Thermal Sciences 63:.
35. PETUKHOV, B . S .

36. Incropera, Frank P. and DeWitt, David P. (2007). Fundamentals of Heat and Mass Transfer (6th ed.). New York: Wiley. p. 514. ISBN 978-0-471-45728-2.
37. Schmidt, E.F. (1967). Wärmeübergang und Druckverlust in Rohrschlangen. Chemie Ingenieur.
38. aeronautics, The Victoria University of Manchester's contributions to the development of.
39. Coulson Richardson Chemical Engineering, Volume 6, Third edition.
40. *Geothermal capacity | About BP | BP Global, Bp.com, retrieved 2014-11-15.*